Enhanced hydrological modeling with the WRF-Hydro lake/reservoir module at Convection-Permitting scale: a case study of the Tana River basin in East Africa

Ling Zhang[1,3,4], Lu Li[2], Zhongshi Zhang[2,3,4], Joël Arnault[5,6], Stefan Sobolowski[7], Xiaoling Chen[8], Jianzhong Lu[8], Anthony Musili Mwanthi[9,10], Pratik Kad[4], Mohammed Abdullahi Hassan[10], Tanja Portele[6], Harald Kunstmann[5,6], Zhengkang Zuo[11]

[1]College of Urban and Environmental Sciences, Hubei Normal University, Huangshi 435002, China.
[2]NORCE Norwegian Research Centre, Bjerknes Centre for Climate Research, Bergen 5007, Norway.
[3]Centre for Severe Weather and Climate and Hydro-geological Hazards, Wuhan 430074, China.
[4]Department of Atmospheric Science, School of Environmental Studies, China University of Geosciences, Wuhan 430074, China.
[5]University of Augsburg, Institute of Geography, Germany.
[6]Karlsruhe Institute of Technology, Institute of Meteorology and Climate Research, Garmisch-Partenkirchen, Germany.
[7]Geophysical institute, University of Bergen and the Bjerknes Center for Climate Research, Bergen, Norway.
[8]State Key Laboratory of Information Engineering in Surveying, Mapping and Remote Sensing, Wuhan University, Wuhan 430079, China.
[9]University of Nairobi, Kenya.
[10]IGAD Climate Prediction and Applications Center, Nairobi, Kenya.
[11]College of Geosciences and Surveying Engineering, Taiyuan University of Technology, No. 18 Xinkuangyuan Road, Taiyuan, 030024

Correspondence to: Lu Li (luli@norceresearch.no); Zhongshi Zhang (zhongshi.zhang@cug.edu.cn)

Abstract. East Africa frequently experiences extreme hydrological events, such as droughts and floods, underscoring the urgent need for improved hydrological simulations to enhance prediction accuracy and mitigate losses. A major challenge lies in the limited quality of precipitation data and constraints in model capabilities. To address these challenges, the upper and middle Tana River basin, characterized by its sensitivity to drought, vulnerability to flooding, and data availability, was selected as a case study. We performed convection-permitting (CP) regional climate simulations using the Weather Research and Forecasting (WRF) model and conducted hydrological simulations by a lake/reservoir-integrated WRF Hydrological modeling system (WRF-Hydro) driven by the CPWRF outputs. Our results show that the CPWRF-simulated precipitation outperforms ERA5 when benchmarked against IMERG, with evident bias reduction in seasonal precipitation mainly over Mount Kenya region and in light rainfall (1-15 mm day^{-1}) probability during the dry season. This improved precipitation enhances the hydrological simulation, significantly reducing false peak occurrences and increasing the Nash-Sutcliffe Efficiency (NSE) by 0.53 in the calibrated lake-integrated WRF-hydro model (LakeCal) driven by CPWRF output compared to ERA5-driven simulations. Additionally, the lake/reservoir module increases the sensitivity of river discharge to spin-up time and affects discharge through lake/reservoir-related parameters, although adjustments to the parameters (i.e. runoff infiltration rate, Manning's roughness coefficient, and the groundwater component) have minimal effects on discharge particularly during the dry season. The inclusion of the lake/reservoir module effectively reduces the model-data bias in WRF-Hydro simulations, particularly for the dry season flow and peak flow, resulting in an NSE increase of 1.67 between the LakeCal and LakeNan (model without lake/reservoir module). Notably, 24 % of the NSE improvement is attributed to CPWRF and 76 % to the lake/reservoir module. These findings highlight the enhanced capability of hydrological modelling when combining CPWRF simulations with lake/reservoir module, providing a valuable tool for improving flood and drought predictability in data-scarce regions like East Africa.

1. Introduction

The credibility of hydrological simulations in data-scarce regions is challenged by the limited quality of precipitation data (e.g., incomplete, unreliability, and poor in-suit coverage) and the constrained capacity of the hydrological model given the underlay's complexities. To make well-informed decisions concerning flood/drought adaptation and loss mitigation, elected officials, planners, and the public require relatively reliable information on flood and drought forecasts, which rely on skilled hydrological simulations. This issue could be particularly acute in drought/flood-prone and vulnerable areas such as East Africa. The economy and population in East Africa mainly depend on rain-fed agriculture and pastoralism, which suffers from frequent droughts and floods (Taye and Dyer, 2024). For example, the drought of 2022 triggered an exceptional food security crisis in Ethiopia, Somalia, and Kenya, pushing more than 20 million people into extreme hunger (NASA, 2022). Similarly, the flood in 2023 here killed more than 100 people and displaced over 700,000 (NASA, 2024). The highlighted risk in East Africa urges effective hydrological simulation for better hydrological extreme forecasts, thus supporting effective water resource planning and management, and aiding informed decision-making and loss mitigation for officials, planners, and the public.

Obtaining even the present-day precipitation, especially in mountainous regions, is challenging due to poor in-situ coverage, and incomplete or unreliable records. Such data scarcity even complicates the evaluation of model output (Li et al., 2017). This issue is only further exacerbated as grid-spacing is decreased to km scales. Gridded precipitation productions tried to be an alternative to address some of the data scarcity issues. These gridded products include merged data such as Climate Hazards Group InfraRed Precipitation with Station data (CHIRPS) (Funk et al., 2015), reanalysis data like ERA-Interim (Dee et al., 2011), and satellite-based data involving Tropical Rainfall Measuring Mission (TRMM) (Adjei et al., 2015) and Integrated Multi-satellite Retrievals for GPM (IMERG) (Dezfuli et al., 2017). However, these products present uncertainties, such as false detection of precipitation events and biases of precipitation amounts (Bitew and Gebremichael, 2011; Ma et al., 2018; Dezfuli et al., 2017) which limit their suitability in the hydrometeorological application. These uncertainties are particularly pronounced in mountainous regions (Li et al., 2018; Maranan et al., 2020; Zandler et al., 2019). Also, precipitation from coarse-resolution Global Climate Models has its limitations (Monsieurs et al., 2018; Kad et al., 2023), primarily due to the model configuration, such as resolution and parameterization, which are crucial for a more realistic representation of processes (Kad et al., 2023; Tao et al., 2020).

Dynamical downscaling models offer a promising tool for generating precipitation patterns with the realistic regional detail. It can capture refine-scale features such as topography and local processes that influence orographic effects (Kad and Ha, 2023; Tao et al., 2020). The study by Kerandi (2017) highlights the importance of using higher-resolution models for more accurate climate features. The WRF model with a refined resolution of 25 km captures the temporal variability on interannual to annul scales, and the spatial distribution of precipitation in the Tana River basin is more effectively represented than the coarser 50 km resolution. Indeed, at relatively coarse resolution (such as >20 km resolution), RCMs generally struggle to adequately represent precipitation and exhibit uncertainties when compared to reanalysis data, rain gauges, and satellite observations (Biskop et al., 2012; Ji and Kang, 2013). A refined horizontal resolution can significantly improve precipitation simulation over Equatorial East Africa (Pohl et al. 2011).

Convection-permitting regional climate models (CPRCMs, typically with a resolution of < 5 km) provide an explicit representation of convection, allowing for capturing local-scale precipitation extremes. This is a clear advantage over the coarser resolutions (Kendon et al., 2021; Schwartz, 2014; Weusthoff et al., 2010). The added value of CPRCMs compared to the parametrized regional climate models includes improved representations of the intensity distribution (Senior, 2021; Berthou et al., 2019), diurnal cycle (Stratton et al., 2018), and storm size and duration (Crook et al., 2019). It is noteworthy that CPRCMs better capture surface heterogeneities and produce more realistic climate simulations over mountainous regions (Kawase et al., 2013; Rasmussen et al., 2014). Furthermore, CPRCMs show increased performance over Africa (Senior, 2021), in presenting rainy events, diurnal cycle, and peak time for the Lake Victoria Basin of East Africa (Lipzi et al. 2023), as well as sub-daily rainfall intensity distribution, especially those related to the convective rainfall in the tropics (Folwell et al. 2022). Therefore, CPRCM holds promise for generating more realistic precipitation with regional details in East Africa.

Atmosphere-hydrological modeling is a common approach for simulating and predicting climate extremes such as floods and droughts. While regional climate model (RCM) outputs are often directly used in hydrological studies, they may introduce inconsistency due to mismatches in spatial and temporal scales or biases in the simulated atmospheric processes (Chen et al., 2011; Teutschbein and Seibert, 2012). A better approach would be to couple atmospheric and hydrological modeling systems to ensure physical consistency. A coupling of the Weather Research and Forecasting Model (WRF) and the WRF hydrological modeling system (WRF-Hydro; Gochis et al., 2018) shows advantages in hydrology simulations and forecasting hydrological extremes globally (e.g., Kerandi et al., 2018; Li et al., 2017), including urban flood prediction over the Dallas-Fort Worth area of North America (Nearing et al. 024) and drought estimation in South Korea (Alavoine and Grenier 2023). In Africa, WRF-Hydro has also proven useful for discharge simulations in the Ouémé River of West Africa (Quenum et al. 2022) and the Tana River basin (Kerandi et al. 2018). Kerandi’s study demonstrated minimal differences in precipitation between the stand-alone and fully coupled models, which suggests that precipitation recycling and land-atmosphere feedback have a limited impact on soil moisture and discharge in the Tana River basin. Similar findings have been observed in other regions, such as the Crati River basin in Southern Italy (Senatore et al., 2015) and the United Arab Emirates (Wehbe et al., 2019).

Although WRF-Hydro shows potential, its application in East Africa requires refinement through the implementation of more comprehensive hydrological processes. Numerous reservoirs have been constructed in East Africa (Palmieri et al., 2003), altering the magnitude and timing of natural streamflow. These reservoirs typically attenuate and delay flows during the rainy season while releasing water during the dry season (Zajac et al., 2017; Hanasaki et al., 2006). Incorporating lakes/reservoir processes in hydrological simulation is essential for creating reliable models in regions with lakes (Hanasaki et al., 2006; Lehner et al., 2011). However, only a few hydrological simulations over East Africa are related to lakes (Oludhe et al., 2013; Naabil et al., 2017; Siderius et al., 2018), and even fewer studies have examined the impact of reservoirs in this region, particularly in cases where meteorological and hydrological models are coupled. Naabil (2017) used WRF-Hydro with the dam-water-balance model for dam-level simulation and water resource assessment in the Tono dam basin, but did not include the reservoir module in the WRF-Hydro system, limiting the accurate capture of the dam's impact on discharge and other hydrological variables. Therefore, hydrological modeling coupled with its lake/reservoir module is required for reliable flood and drought simulations over East Africa. While the WRF-Hydro system, integrated with the lake/reservoir module, shows promise for simulating the water balance affected by reservoirs (Maingi and Marsh, 2002), its use in East Africa, especially in large river basins like the Tana River, remains limited.

The Tana River basin in East Africa is ideal for enhanced hydrological modeling due to its proneness and vulnerability to droughts and floods, as well as the availability of observational data. These discharge records provide a benchmark for simulations despite some uncertainties. The basin supports vital ecosystem services for Kenya, including drinking water supply, hydroelectric power generation, agriculture, and biodiversity, and is home to over eight million people (Lange et al., 2015). However, the region is observed to be at risk of drought and flood, which are likely exacerbated by climate change (Kenya Climate Change Case Study, 2024). Droughts occur approximately every five years, causing water shortages for drinking water, irrigation, and fishing (Bonekamp et al., 2018). The 2018 flood overflowed the riverbanks, damaging crops, homes, and infrastructure, displacing thousands of people, and contributing to outbreaks of waterborne diseases such as cholera (Kiptum et al., 2024). Robust hydrological modeling in the Tana River basin is essential for accurate predictions of extreme events and practical risk assessment. Using the Tana River basin as a case study, our research aims to address some of the issues related to flood and drought risk mitigations, through a more comprehensive hydrological simulation with a convection-permitting WRF model and lake/reservoir-integrated WRF-Hydro system. We target the following sub-objectives: (1) to improve climate output (particularly focusing on precipitation) through convection-permitting (CP) WRF simulation (CPWRF) and using the enhanced precipitation representation to advance the hydrological simulation; (2) to explore the potential of lake/reservoir module to improve the hydrological simulation skill; (3) to build an enhanced WRF-Hydro system and investigate the contribution of (1) CPWRF simulation and (2) lake/reservoir module to hydrological simulation improvement. The research aims to improve hydrological models, which helps to better water resource management and risk mitigation, and supports sustainable practices in regions vulnerable to water-related damages.

2. Study area and data

The Tana River Basin, located in the tropics, exhibits dual peaks in precipitation due to the biannual migration of the Intertropical Convergence Zone (ITCZ). The spatial distribution of the precipitation is profoundly modulated by the basin's varied topography and atmospheric deep convection (Kad et al., 2023; Johnston et al., 2018), which results in a gradient condition ranging from arid in the lowlands to semi-humid in the highlands and coastal areas (Knoop et al., 2012). The precipitation pattern is also influenced by El Niño/Southern Oscillation (Otieno and Anyah, 2013; Anyah and Semazzi, 2006), IOD (Williams and Funk, 2011), and rising atmospheric CO2 (Kad et al., 2023).

Our study focuses on the upper and middle Tana River Basin (TRB), covering an area of 32,865 km² upstream of Garissa city (S 1.25°-N 0.50°, E 36.50°-E 39.75°). This region includes famous mountain ranges, such as the Mount Kenya massif and the Aberdare Range, alongside plain surfaces (Fig. 1 b). The region is characterized by a complex interplay between mountainous terrain and flat surface, with elevation ranging from 34 meters to excess of 4800 (Fig. 1 a). To analyze and evaluate the spatial distribution of precipitation concerning the topography, we classified the terrain into mountainous regions above 1,600 meters and plains below 1,600 meters. There are five reservoirs in the basin along the Tana River, including Masinga, Kamburu, Gitaru, Kindaruma, and Kiambere from the upstream to downstream (Table 1, Fig. 1 c). These five lakes are between Garissa station upstream and Rukanga downstream. It is important to note that the lakes don't affect the streamflow at Rukanga, but they do impact the discharge at Garissa.

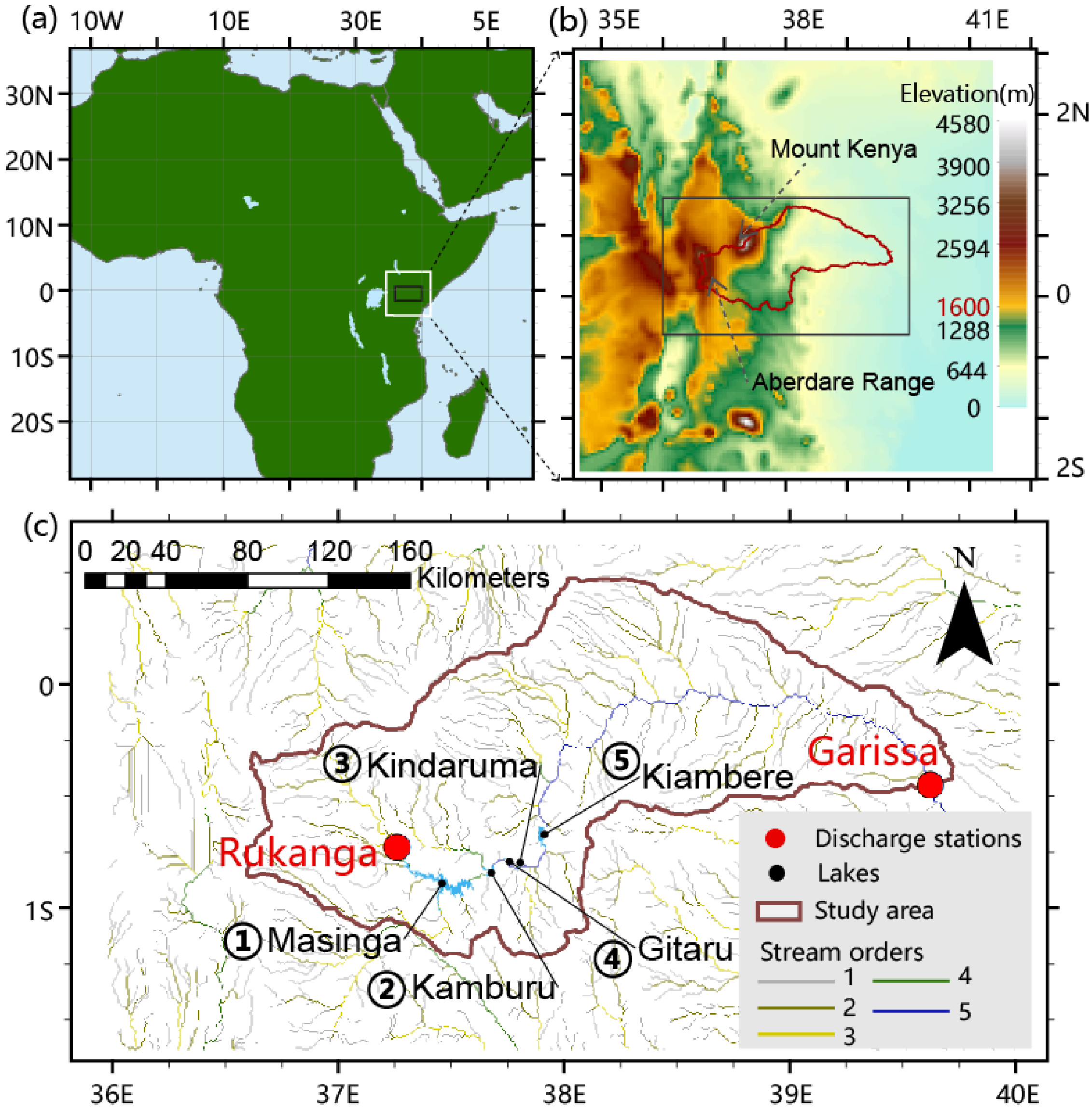

Figure 1. Study basin location in East Africa. (a) The WRF domain with a resolution of 5 km (shown with the white frame) and the location of the inner region (a black frame) used as the domain of WRF-Hydro simulation (b) A zoomed view of the inner area showing topography, two major mountains, and the basin boundary. (c) Drainage map of the upper and middle Tana River Basin, including the discharge stations, lake/reservoir water level stations, and the stream orders for hydrological modeling in the WRF-Hydro model system.

Table 1. Lakes in the upper and middle Tana River basin (TRB).

Name	Water level (max/min; unit: m）	Water depth (m)	Area (km^2)	Operating date
KAMBURU	1007/996	1007	11.7	1974
KINDARUMA	781/775	7811	2.1	1981
MASINGA	1058/1035	1058	111.6	1981
GITARU	925/917	9255	2.7	1978
KIAMBERE	702/681	702	23.2	1981

Here, we used a global satellite product of GPM_3IMERGDF (GPM IMERG precipitation version 6 at daily temporal resolution and 0.1° x 0.1° spatial resolution) (Huffman et al., 2020) for CPWRF precipitation evaluation, downloaded from the NASA website (https://gpm.nasa.gov/data-access/downloads/gpm, accessed on 28 Apr 2023). These climate data cover the period 2010-2014.

Discharge observations during 2011-2014 at two stations in TRB (Garissa and Rukanga), obtained from the Water Resources Authority of Kenya (WRA), are used for WRF-Hydro model discharge sensitivity analysis and calibration (Fig. 1).

3. Methodology

3.1. WRF domain design for convection-permitting modeling

To obtain convection-permitting regional climate model simulations, we used the Advanced Research WRF (WRF-ARW) model of version 4.4 (Skamarock et al., 2019) with the designed domain of 5 km spatial resolution (Fig. 1). The lateral boundaries were forced with the 6-hourly ERA5 reanalysis with a spatial resolution of 0.25 degrees (Hersbach et al., 2020). The model was set with 50 vertical levels up to 10 hPa. The convection parameterization was turned off for the CPWRF simulation, the Mellor-Yamada Nakanishi Niino Level 2.5 (MYNN2.5) Scheme (Nakanishi and Niino, 2006) for the planetary boundary layer, the RRTM scheme for longwave radiation (Mlawer et al., 1997), and the Dudhia Shortwave scheme for shortwave radiation (Jimy Dudhia, 1989). The Noah-MP Land Surface model ('Noah-MP LSM', Yang et al., 2011) was used for the land surface scheme.

The model runs from 1 January 2010 to 31 December 2014. Typically, WRF simulations require a spin-up of about one month, which should ideally be excluded from precipitation evaluation. However, given the limited length of simulated precipitation, the subsequent analysis is based on full precipitation simulation from January 2010 to December 2014.

3.2. Sensitivity analysis and calibration strategy for WRF-Hydro modeling

3.2.1. WRF-Hydro modeling and preliminary calibration

For hydrological modeling, the WRF-Hydro system of version 5.3 (Gochis et al., 2018) was employed in an offline mode, driven by the CPWRF atmospheric data within a domain at 5 km resolution with 90×50 pixels over the TRB (Fig. 1). The sub-grid routing processes were executed at a 500 m grid spacing and surface physiographic files were generated by ArcGIS 10.6 (Sampson and Gochis, 2015). The physiographic files included high-resolution terrain grids (that specified the topography), channel grids, flow direction, stream order (for channel routing), a groundwater basin mask, and the position of stream gauging stations. The first five stream orders and gauging stations are shown in Fig. 1 c. We activated the saturated subsurface overflow routing, surface overland flow routing, channel routing, and base-flow modules. The overland flow routing and channel routing were calculated by a 2-D diffusive wave formulation (Julien et al., 1995) and a 1-D variable time-stepping diffusive wave formulation, respectively.

The model involves the five lake/reservoirs using a level-pool lake/reservoir module, which calculates both orifice and weir outflow. Fluxes into a lake/reservoir object occur when the channel network intersects a lake/reservoir object. The level-pool scheme tracks water elevation over time, and water exits the lake/reservoir either through weir overflow ($Outflow_w$) or orifice-controlled flow ($Outflow_o$), as described by Eq. (1) and (2).

$$Outflow_w = \begin{cases} C_w L h^{3/2}, h > h_{max} \\ 0, h \leq h_{max} \end{cases} \tag{1}$$

where h is the water elevation (m), h_{max} is the maximum height before the weir begins to spill (m), C_w is the weir coefficient, and L is the length of the weir (m).

$$Outflow_o = C_o S_o \sqrt{2gh} \tag{2}$$

where C_o is the orifice coefficient, S_o is the orifice area (m^2), and g is the acceleration of gravity ($m\ s^{-2}$).

For the sensitivity analysis and model optimization, we initially calibrated the WRF-Hydro system without the lake/reservoir (with the lake/reservoir module inactive). Two key hydrological parameters, REFKDT and MannN, were tuned using the auto-calibration Parameter Estimation Tool (PEST, http://www.pesthomepage.org). The optimization is performed by maximizing the accuracy of the discharge simulation, indicated by the Nash-Sutcliffe Efficiency (NSE) coefficient (Nash and Sutcliffe, 1970) of simulated discharge against the observation at Garissa. The calibrated WRF-Hydro model without the lake/reservoir is referred to as LakeNan in the following analysis.

3.2.2. Experiments designed for sensitivity analysis in WRF-Hydro modeling with lake/reservoir module

To optimize WRF-Hydro modeling over TRB, we facilitated a comprehensive sensitivity analysis, involving spin-up time, hydrological parameters, groundwater components, and lake/reservoir-related parameters. Groundwater component tunning focuses on the parameter GWBASEWCTRT (an option for groundwater mode). Hydrological parameters include the Manning roughness parameter (MannN) and runoff infiltration coefficients (REFKDT). Lake/reservoir-related parameters cover the elevation of the maximum lake/reservoir height (LkMxE, unit: m), weir elevation (WeirE, unit: m), weir coefficient (WeirC, ranging from zero to one), weir length (WeirL, unit: m), orifice area (OrificeA, unit: m^2), orifice coefficient (OrificeC, ranging from zero to one), orifice elevation (OrificeE, unit: m), and lake/reservoir module area (LkArea, unit: m^2).

For sensitivity analysis of specific parameters, a set of experiments were conducted. In each experiment, only the parameter of interest was changed while all others were kept at their defaults (Table 2). The defaults of lake/reservoir-related parameters were obtained from the WRF-Hydro GIS pre-processing toolkit (Gochis et al., 2018), while the others were derived from the preliminary calibrated WRF-Hydro system without lake/reservoir module (LakeNan, Sect. 3.2.1).

Table 2. The default values for sensitivity experiments.

Group	Parameters	The default value
Spin-up	Spin-up time	restart with a 10-year spin-up time, using the initial condition from a 10-year simulation covering January 2005 to December 2014.
Hydrological parameters	REFKDT	5
	MannN	(0.55,0.35,0.15,0.1,0.07, 0.05, 0.04, 0.03, 0.02, 0.01) for the ten stream orders
Groundwater	GWBASEWCTRT	“GWBASESWCRT_Sink” for sensitivity tests of spin-up and hydrological parameters; “GWBASESWCRT_Passthrough” for sensitivity tests of lake/reservoir-related parameters, and the subsequent calibration.
Lake/reservoir-related parameters	LkMxE	-9,957,781,074,917,690
	WeirE	(990.5,775.9,1067.9,915.3,689.1)
	WeirC	(0.4,0.4,0.4,0.4,0.4)
	WeirL	(10,10,10,10,10)
	OrificeA	(1,1,1,1,1）
	OrificeC	(0.1,0.1,0.1,0.1,0.1)
	OrificeE	(965,764,1033.3,905.7,644.3)
	LkArea	(11.7,2.1,111.6,2.7,23.2)

The default values for REFKDT and MannN are from the preliminary calibration of the LakeNan model (WRF-Hydro system without lake/reservoir module). The MannN value is different for each stream order from 1 to 10. (Value1, Value2, Value3, Value4, Value5) indicate value for the five reservoirs (KAMBURU, KINDARUMA, MASINGA, GITARU, KIAMBERE), obtained from WRF-Hydro GIS pre-processing toolkit. Two options for the groundwater component were involved in the experiments. Groundwater component with “GWBASESWCRT_Sink” option creates a sink at the bottom of the soil column, where water draining from the column exits the system into the sink. The "GWBASESWCRT_Passthrough" option bypasses the bucket model, directly transferring all flow from the bottom of the soil column into the channel.

Sensitivity to spin-up time

To obtain a stable hydrological simulation, a spin-up time is required. Insufficient spin-up for initialization can introduce unnecessary uncertainties, potentially compromising the accuracy of subsequent sensitivity analyses and hydrological modeling assessments. Previous studies have demonstrated that spin-up time influences initial conditions such as the soil moisture content, surface water, lake/reservoir module water level, and groundwater, which potentially influences the fidelity of model simulations (Ajami et al., 2014a; Ajami et al., 2014b; Bonekamp et al., 2018; Seck et al., 2015), and subsequently affect the result of subsequent sensitivity analyses and the performance of the hydrological simulation. For example, groundwater simulation may require more than 10 years of spin-up to reach stability (Ajami et al., 2014a). Since the shortest spin-up time likely depends on the quality of the model input (especially soil data) and local conditions, the impact of the spin-up time needs to be assessed on a case-by-case basis. Therefore, we first investigated the sensitivity of spin-up time to identify the shortest duration required for achieving model stability and ensuring computational efficiency.

In our study, we conduct experiments of 17 different spin-up times (Table 3) to examine their impacts on peak flow and average discharge in TRB, for both WRF-Hydro systems with the lake/reservoir module (LakeRaw) and without it (LakeNan). To analyze the sensitivity of peak flow, we initialized the simulations on the observed Peak-Flow day (26 November 2011) with varying spin-up times ranging from 1 day to 12 years. In the spin-up experiments, the restart date precedes 1 January, 2010, which is not available in the WRF drivers. Therefore, we use data from 2010 as a substitute for the driving climate of each preceding year (i.e. 2000, 2001,…,2009). In all LakeRaw experiments, the parameters are set as their defaults, as shown in Table 2.

Table 3. Overview of 17 spin-up time experiments

Experiment name	Restart date	Spin-up time
1 day spin-up	25 November 2011	1 day
3 mon spin-up	26 August 2011	3 months
6 mon spin-up	26 May 2011	6 months
9 mon spin-up	26 February 2011	9 months
1 year spin-up	26 November 2010	1 year
15 mon spin-up	26 August 2010	15 months
18 mon spin-up	26 May 2010	18 months
21 mon spin-up	26 February 2010	21 months
3 year spin-up	1 January 2009	3 years
4 year spin-up	1 January 2008	4 years
5 year spin-up	1 January 2007	5 years
6 year spin-up	1 January 2006	6 years
7 year spin-up	1 January 2005	7 years
8 year spin-up	1 January 2004	8 years
9 year spin-up	1 January 2003	9 years
10 year spin-up	1 January 2002	10 years
11 year spin-up	1 January 2001	11 years
12 year spin-up	1 January 2000	12 years

The initialization time for one model to reach equilibrium was calculated as the duration required for the temporal changes of the model output variable to decrease to a specific threshold value (Cosgrove et al., 2003). In our study, this threshold value was set as half the standard deviation of the last experiments (i.e. 9, 10, 11, and 12-year spin-up experiments) for a specific variable. The temporal changes were measured as the difference of the variable between the two adjacent experiments.

Sensitivity to hydrological parameters

The parameters of MannN and REFKDT have been demonstrated to influence the simulated river discharge significantly (Ryu et al., 2017; Yucel et al., 2015), which were selected for the sensitivity test. For each test, the parameter values range from the minimum to the maximum, generating ten values with nearly equal intervals and resulting in ten experiments (Table 4). For MannN, which must be larger than 0, the minimum scaling is set to 0.1 instead of 0.

Table 4. Sensitivity analysis (SA) experiments designed for REFKDT.

Experiments for REFKDT SA	Value
REFKDT_1	0.02*default
REFKDT_2	0.13*default
REFKDT_3	0.24*default
REFKDT_4	0.35*default
REFKDT_5	0.46*default
REFKDT_6	0.56*default
REFKDT_7	0.67*default
REFKDT_8	0.78*default
REFKDT_9	0.89*default
REFKDT_10	1*default

Note: The default is obtained from the WRF-Hydro GIS pre-processing toolkit. * indicates multiplication.

Table 5. Sensitivity analysis (SA) experiments designed for MannN of the first five stream orders.

Experiments for MannN SA	Value
MannN_1	0.1*default
MannN_2	0.44*default
MannN_3	0.89*default
MannN_4	1.33*default
MannN_5	1.78*default
MannN_6	2.22*default
MannN_7	2.67*default
MannN_8	3.11*default
MannN_9	3.56*default
MannN_10	4.00*default

Note: The default is obtained from the WRF-Hydro GIS pre-processing toolkit. * indicates multiplication.

Sensitivity to groundwater component

We investigate the sensitivity of groundwater components by tunning GWBASWCTRT, with two options in two experiments. Groundwater component with "GWBASESWCRT_Sink" option creates a sink at the bottom of the soil column, where water draining from the column exits the system into the sink. The "GWBASESWCRT_Passthrough" option bypasses the bucket model and directly transfers all flow from the bottom of the soil column into the channel. It's important to note that with the option "GWBASESWCRT_Sink", water draining from the bottom of the soil column will not achieve water balance closure.

Sensitivity to lake/reservoir parameters

Morris method (Morris, 1991) was employed to analyze the sensitivity of the seven lake/reservoir-related parameters, due to its low computational cost and ease of interpretation (Wei, 2013). This method is widely used in global sensitivity analysis in hydrological models, especially in computationally expensive models (Song et al., 2013; Wei, 2013). In the study, the sensitivity analysis was simultaneously conducted on the five lakes to reduce computational cost. In the Morris experiment, the eight main lake/reservoir-related parameters of the five lakes were normalized to a range of 0-1, by subtracting the minimum value and dividing by the maximum minus the minimum (Table 5). Based on the eight normalized values with a lower value of zero and an upper of one, we generated all samples for Morris screening. The number of replications R, level p, and sample size N were set as 10, 4, and 90 (i.e. 90 parameter sets for 90 runs), respectively. For each sample, corresponding to a WRF-Hydro simulation, the eight parameters for each lake/reservoir were inverse-normalization. The other parameters were kept as their defaults. Two metrics were generated to examine the sensitivity: order of importance (u* in Fig. 8) and dependencies with other parameters (σ/u* in Fig. 8). The u* of a specific parameter with a higher value indicates greater sensitivity. The large value of σ/u* indicates stronger dependencies with other parameters.

Table 6. Sensitivity analysis experiments designed for the 8 lake/reservoir-related parameters.

Parameters	Value_min	Value_max
OrificeC	0.01*default	10*default
WeirL	0.01*default	1.2*default
WeirC	0.001*default	0.25*default
OrificeA	0.001*default	1000*default
Dam_Length	0.001*default	20*default
LxMkE	Wlmax-Wd*0.5	Wlmax+Wd*0.5
WeirE	OrificeE_default	Wlmax+Wd*0.5
OrificeE	Wlmin*0.5	Wlmin

Note: Wlmax, Wlmin, Wd, and OrificeE_default indicate the max water level, min water level, water depth, and OrificeE default value, respectively. The default is obtained from the WRF-Hydro GIS pre-processing toolkit.

We also compared the sensitivity of the simulated discharge to lake/reservoir-related parameters across the five lakes. To conserve computational resources, the tests were based on the simulations from the calibration. For each test of parameters related to one lake, more than 30 simulations were conducted. Each simulation related to a given lake involves the seven parameters (LkMxE, WeirE, OrificeE, WeirC, WeirL, OrificeC, and Damlength). In all simulations for the given lake, the values of seven parameters varied synchronously, changing linearly from the minimum to the maximum shown in Table 6.

In the parameter setting, we make some rules to constrain the three parameters (i.e., LkMxE, WeirE, and OrificeE), to make the simulation result reasonable: (1) LkMxE should be larger than both WeirE and OrificeE; (2) OrificeE was suggested to be smaller than WeirE. To satisfy these constraints, the OrificeE is set to be below the minimum water level, WeirE ranges from the OrificeE default value to the maximum water level plus half water depth, and LkMxE changes from the maximum water level minus haft depth to maximum water level plus half depth. Besides, OrificeC and WeirC should be kept between 0 and 1, which should be a constant. The selection of maximum and minimum values, as well as the number of experiments, is flexible, as long as they are reasonable and produce realistic simulations.

3.2.3. Final calibration for WRF-Hydro modeling with lake/reservoir module

Based on the sensitivity analysis, we developed a comprehensive calibration strategy for the WRF-Hydro system incorporating the lake/reservoir module. Building on the preliminary calibration (Sect. 3.2.1), we re-tuned the lake/reservoir-related parameter sets for the five lakes, respectively. Of the lake/reservoir parameter sets, each was calibrated sequentially from upstream to downstream, with more than 30 experimental iterations. Once the upstream lake was calibrated, its parameters were fixed as optimized, and we proceeded to calibrate the parameters set for the next downstream lake. Subsequently, we focused on re-tuning REFKDT and MannN, each subjected to 30 experimental iterations. The parameter sets for each iteration were generated according to Sect. 3.2.2. Throughout this process, we achieved a well-calibrated WRF-Hydro model (LakeCal) with an optimal parameter set, determined by the best NSE value calculated over simulated discharge from January 2011 to December 2014 against the observations at Garissa station. Typically, we should use the same time series for discharge analysis as for the precipitation evaluation (2010-2014). However, since WRF-Hydro requires at least one year of spin-up, the discharge evaluation excludes the first year, focusing instead on the period from 2011 to 2014.

3.3. Peak flow, dry season flow, and rainy season flow

To measure modeling performance, we obtained the flow from the long rainy season of March-May (MAM), the short rainy season of October-December (OND), the dry season of January-February (JF), and June-September (JJAS), as well as the peak flow. The maximum observed daily discharge at Garissa station over 2010-2014 occurred on 26 November 2011 (844 $m^3 s^{-1}$) and is used as a peak flow case (Peak-Flow) for our evaluation. Since the model cannot capture the peak on the exact date, the simulated Peak-Flow was set as the largest daily discharge during the 21 day period centred around the observed Peak-Flow.

3.4. Evaluation of simulated precipitation from CPWRF

To assess whether the CPWAR has advantages over their driving forces (ERA5), added value (AV) proposed by Dosio et al. (2015) was applied, expressed as follows.

$$AV = \frac{(X_{ERA5} - X_{IMERG})^2 - (X_{CPWRF} - X_{IMERG})^2}{\max\left((X_{ERA5} - X_{IMERG})^2, (X_{CPWRF} - X_{IMERG})^2\right)} \quad (3)$$

X_{ERA5}, X_{CPWRF}, *and* X_{IMERG} indicate precipitation from the driving forces (ERA5), CPWRF simulation, and benchmark (IMERG), respectively. The added value (AV) from CPWRF is defined as the performance difference between itself and the driving forces for precipitation in a specific region and period. If the CPWRF adds value compared to the driving forces from ERA5, the AV is positive, whereas a negative AV suggests no adding value.

To fully evaluate the simulated precipitation by CPWRF, we also employed Taylor diagrams (Taylor, 2001), which present a concise statistical summary in terms of spatial correlation (indicated by correlation coefficient), and spatial variance (indicated by normalized standardized deviation). A higher spatial correlation and a spatial variance closer to 1 indicate better simulation skills.

3.5. Attribution of hydrological model improvement to convection-permitting WRF simulation and lake/reservoir module

To assess the contributions of CPWRF simulations and the lake/reservoir module, we compared three models: (1) the calibrated WRF-Hydro model without the lake/reservoir module, driven by CPWRF output (LakeNan), (2) the well-calibrated WRF-Hydro model integrated with the lake/reservoir module, also driven by CPWRF output (LakeCal), and (3) the well-calibrated WRF-Hydro simulation with the lake/reservoir module, driven by ERA5 (LakeCal-ERA5). We calculated the NSE value of simulated discharge against observed data for each model. Next, we computed the NSE increment between LakeCal relative to LakeNan representing improvements due to CPWRF precipitation, and the increment between LakeCal and LakeCal-ERA5 reflecting the influence of the lake/reservoir module. The ratio of CPWRF precipitation-induced or lake/reservoir module-induced NSE increment to the total increment is provided as the attribution of hydrological simulation improvements to the CPWRF simulations or the lake/reservoir module.

4. Results

4.1. WRF Precipitation refinement

Using IMERG precipitation as a benchmark, we evaluated the performance of CPWRF precipitation at a 5 km resolution in TRB, compared to the ERA5 reanalysis, which served as the forcing for our CPWRF simulation. This evaluation focused on seasonal precipitation averaged over 2010-2014 (Fig. 2) and daily precipitation distribution (Fig. 3). Taylor diagram (Taylor, 2001), with spatial correlation (r, correlation coefficient) and spatial variance (normalized standardized deviation), is also applied for evaluation (Fig. S2).

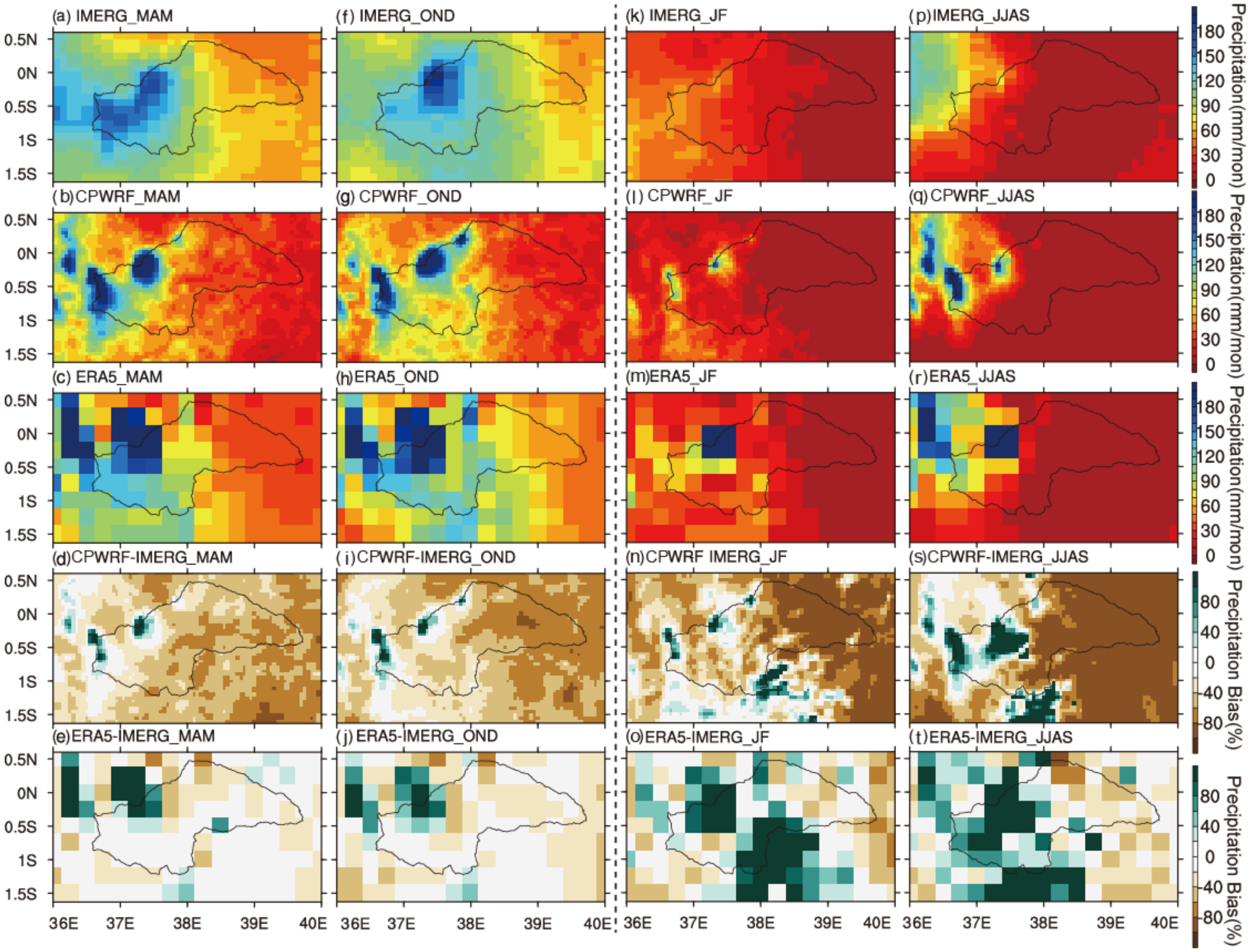

Figure 2. Seasonal precipitation of March-May (MAM, long rainy season, a-c), October-December (OND, short rainy season, f-h), and the JF (January-February, k-m), and JJAS (June-August, p-r) over the upper and middle stream of Tana River Basin (TRB), as well as its bias (d-e, i-j, n-o, and s-t). (a, f, k, p), (b, g, i, q), and (c, h, m, r) indicate IMERG, WRF, and ERA5 data. (d, i, n, s) and (e, j, o, t) donates the bias of CPWRF and ERA5 against IMERG. The seasonal precipitation (MAM, OND, JF, and JJAS) is calculated based on daily data (in March-May, October-December, January-February, and June-August) over 2010-2014. The gray polygon indicates the boundary of the upper and middle sections of the Tana River basin.

Table 7. Seasonal and annual precipitation averaged over the terrain (elevation > 1600 mm) and plain (elevation < 1600 mm) area.

Precipitation (mm)	Mountainous Area					Plain Area				
	Annual	MAM	OND	JF	JJAS	Annual	MAM	OND	JF	JJAS
CPWRF	1393	505	471	87	330	359	153	174	16	17
ERA5	1864	557	603	230	474	593	219	278	48	49
IMERG	1183	457	442	91	193	669	279	326	36	28
CPWRF-IMERG	210(18%)	48(10%)	29(7%)	-5(-5%)	138(72%)	-310(-46%)	-126(-45%)	-152(-47%)	-20(-56%)	-11(-39%)
ERA5-IMERG	681(58%)	100(22%)	161(37%)	139(152%)	281(146%)	-75(-11%)	-61(-22%)	-48(-15%)	12(34%)	22(79%)

Note: Precipitation from IMERG is the benchmark to evaluate that from CPWRF simulation.

The CPWRF model captures the spatial pattern of precipitation and its seasonal variations over TRB, as presented in IMERG (Fig. 2 and Table 7). The spatial distribution of CPWRF simulation reveals that the precipitation is primarily concentrated in mountainous regions, such as Mount Kenya and Aberdare Range, and the surroundings (seen in Fig. 1 b), with significantly less precipitation in the plain area (Fig. 2 b, g, l, and q). The annual mean precipitation is approximately 1500 mm in the mountainous areas compared to less than 500 mm in the plain area (Table 7). During the rainy seasons (MAM and OND), the total precipitation is 976 mm over the terrain area and 327 mm over the plain area, in contrast to 417 mm and 33 mm during the dry season (JF and

JJAS). This spatial and seasonal pattern is consistent with that in IMERG data (Figs 2 a, f, k, and p), indicating a distinct orographic and seasonal dominance.

Compared to ERA5, CPWRF precipitation generally shows better performance, indicated by the Taylor diagram (Fig. S1 e-f) in terms of spatial correlation (correlation coefficient) and spatial variance (normalized standardized deviation) although the advantage is not obvious. The median correlation coefficient of CPWRF precipitation against IMERG is 0.80, higher than ERA5's value of 0.66 (Fig. S1 e). Similarly, the median normalized standardized deviation of CPWRF precipitation is 1.1, closer to 1, compared to ERA5’s value of 1.7 (Fig. S1 f). The improved performance of CPWRF is also evident from the model-data bias comparison. The CPWRF simulation shows a smaller area with large biases (exceeding 60%) compared to ERA5. During MAM, OND, JF, and JJAS, the areas with large biases are 618.2 km^2 (1.9%), 711.0 km^2 (2.2%), 680.0 km^2 (2.1%), and 3431.0 km^2 (10.4%), respectively. In contrast, ERA5 shows corresponding areas of 1545.5 km^2 (4.7%), 1545.5 km^2 (4.7%), 10818.3 km^2 (32.9%), and 8500.1 km^2 (25.9%), respectively.

Spatially, the superior performance of CPWRF precipitation compared to ERA5 merges in the mountainous regions, mainly over Mount Kenya and its surroundings, as demonstrated by the spatial distribution of the model-data bias (Fig. 2 d-e, i-j, n-o, and s-t) and AV (Fig. S2) result. Specifically, the model-data bias from CPWRF is 210 mm (18 %) per year over the mountainous areas, whereas ERA5 shows a bias of 681 mm (58 %) (Table 7). Additionally, over the mountainous areas, CPWRF adds value to ERA5 (Fig. S2 a-e), with a positive AV of 0.14 averaged across the four seasons and this area. Such improvement over the mountainous areas is more pronounced in JF season. Model-data bias in JF season is -5 mm (-5%) from CPWRF and 139 mm (152%) from ERA5. In contrast, during the MAM, OND and JJAS, the bias is 29 mm (7 %), 48 mm (10 %) and 138 mm (72%) from CPWRF with the value of 161 mm (37 %), 100 mm (22 %) and 281 mm (146%) from ERA5. The improvement over the mountainous areas during JF season is highlighted in the Taylor diagram (Fig. S1 c). The spatial correlation or normalized standardized deviation, calculated over the JF averaged precipitation in the mountainous areas, is 0.56 or 2.18 for CPWRF, in contrast with -0.14 or 5.46 for ERA5.

Also, the probability distribution of regionally averaged daily precipitation from CPWRF result exhibits better alignment with the benchmark than from ERA5 (Fig. 3). The CPWRF aligns more closely with IMERG for both small (0-20 mm/day) and extreme (>20 mm/day) rainfall events compared to ERA5, as shown in Fig. 3 and Table 8. The cumulative probability of the small (or extreme) rainfall is 0.991 (0.009) from CPWRF and 0.981 (0.019) from IMERG, whereas 0.995 (0.005) from ERA5. Among these, the better alignment of light rainfall (1-15 mm day^{-1}) probability between CPWRF and IMERG is pronounced (Fig. 3 and Table 8). The probability of light rainfall from CPWRF is 0.255, and 0.242 from IMERG, whereas 0.489 from ERA5. Consistently, CPWRF adds value to ERA5 over the probability of light rainfall (Fig. S2 f-k), with a positive AV of 0.21 averaged across the basin during the four seasons. The better alignment of light rainfall from CPWRF than ERA5 is particularly evident during the dry season (Fig. 3). The probability of 1-15 mm day^{-1} events during the dry season from CPWRF is 0.15 and 0.13 from IMERG, whereas 0.32 from ERA5.

Table 8. Cumulative distribution of daily precipitation regionally averaged over TRB, from CPWRF simulation, IMERG, and ERA5.

Precipitation (mm day^{-1})	Whole period			Dry period			Wet period		
	IMERG	CPWRF	ERA5	IMERG	CPWRF	ERA5	IMERG	CPWRF	ERA5
0–20	0.981	0.991	0.995	0.999	0.999	0.999	0.962	0.982	0.991
>20	0.019	0.009	0.005	0.001	0.001	0.001	0.038	0.018	0.009
1–15	0.255	0.242	0.489	0.126	0.146	0.317	0.381	0.337	0.658

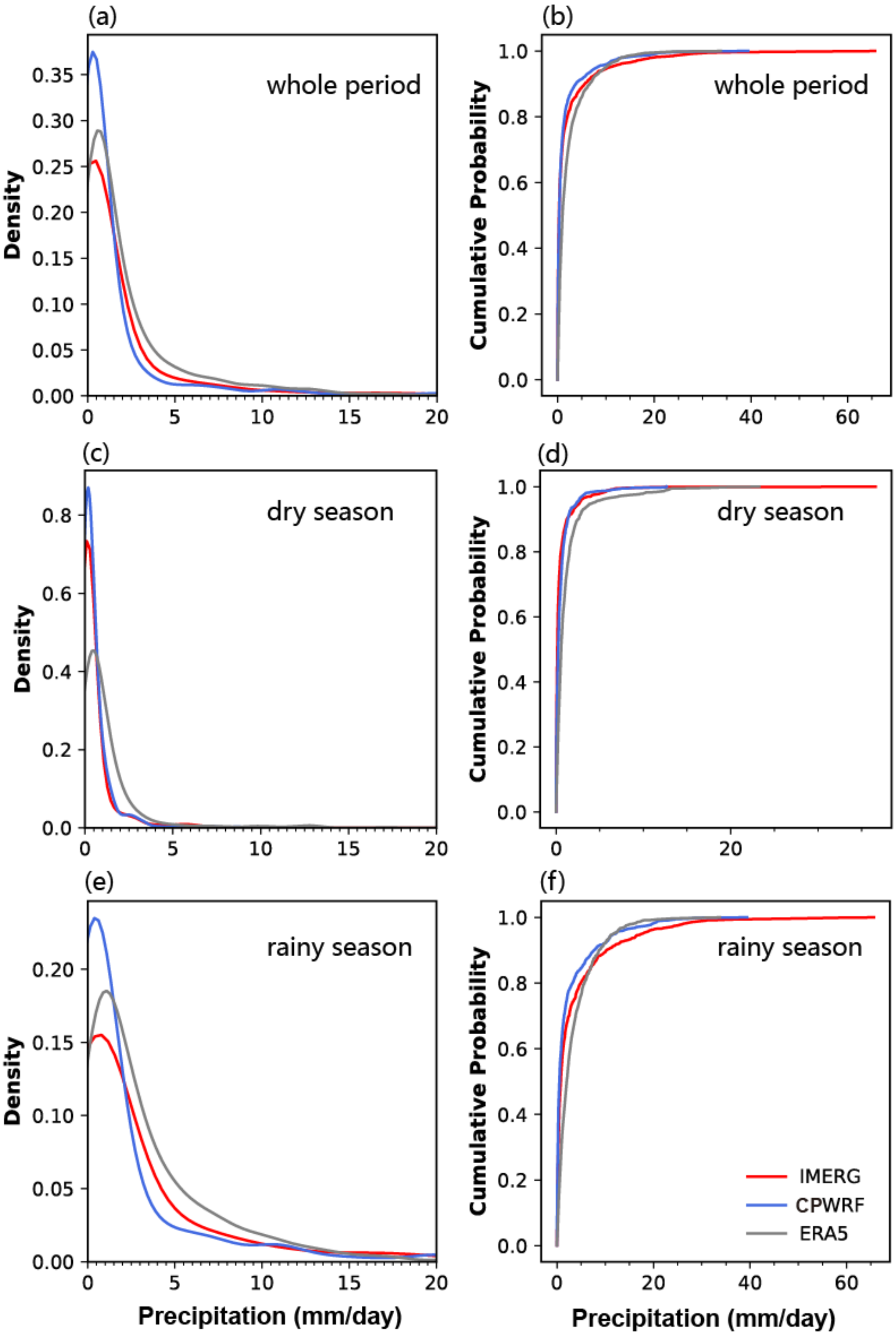

Figure 3. The distribution (a, c, and e) and cumulative distribution (b, d, and f) of daily precipitation from CPWRF result (blue), ERA5 (grey), against the IMERG (red, 2010-2014) over the whole period, dry season and rainy season. (a, b), (c, d) and (e, f) indicate the daily precipitation distribution over the whole period, dry season, and rainy season, respectively.

Table 8. Cumulative distribution of daily precipitation regionally averaged over TRB, from CPWRF simulation, IMERG, and ERA5.

Precipitation	Whole period			Dry period			Wet period		
(mm day^{-1})	IMERG	CPWRF	ERA5	IMERG	CPWRF	ERA5	IMERG	CPWRF	ERA5
0–20	0.981	0.991	0.995	0.999	0.999	0.999	0.962	0.982	0.991
>20	0.019	0.009	0.005	0.001	0.001	0.001	0.038	0.018	0.009
1–15	0.255	0.242	0.489	0.126	0.146	0.317	0.381	0.337	0.658

4.2. WRF-Hydro model optimization with lake/reservoir module

4.2.1. A preliminary investigation of the lake/reservoir impact on discharge

To assess the impact of the lake/reservoir module on hydrological simulation, we compared simulated discharges from different WRF-Hydro modeling experiments against the observations. These experiments included WRF-Hydro with the lake/reservoir module (LakeRaw) and without it (LakeNan), as shown in Fig. 4. The evaluation results (including KGE, Bias, r^2 and NSE) from all these experiments are presented in Table S2. The WRF-Hydro model with lake/reservoir module (LakeRaw) improves discharge simulation compared with that without it (LakeNan), even without model calibration. LakeRaw achieved an NSE of 0.01 and a bias of 40 %, compared to -1.09 and -53 % from the LakeNan. The inclusion of the lake/reservoir module addresses the underestimation of dry season flows. However, the lake/reservoir module (in the LakeRaw) tends to induce overestimation, particularly during February-March and August-September, contributing approximately 81 % of the annual average dry season flows. This overestimation in LakeRaw is likely due to uncalibrated parameters, including spin-up time, the hydrological parameters, groundwater component, and lake/reservoir-related parameters. The hydrological parameters, groundwater component and lake/reservoir-related parameters need to be further adjusted when the lake/reservoir is included in WRF-Hydro system. To enhance the performance of WRF-Hydro modeling with lake/reservoir module, the sensitivity and optimization potential of these parameters were investigated.

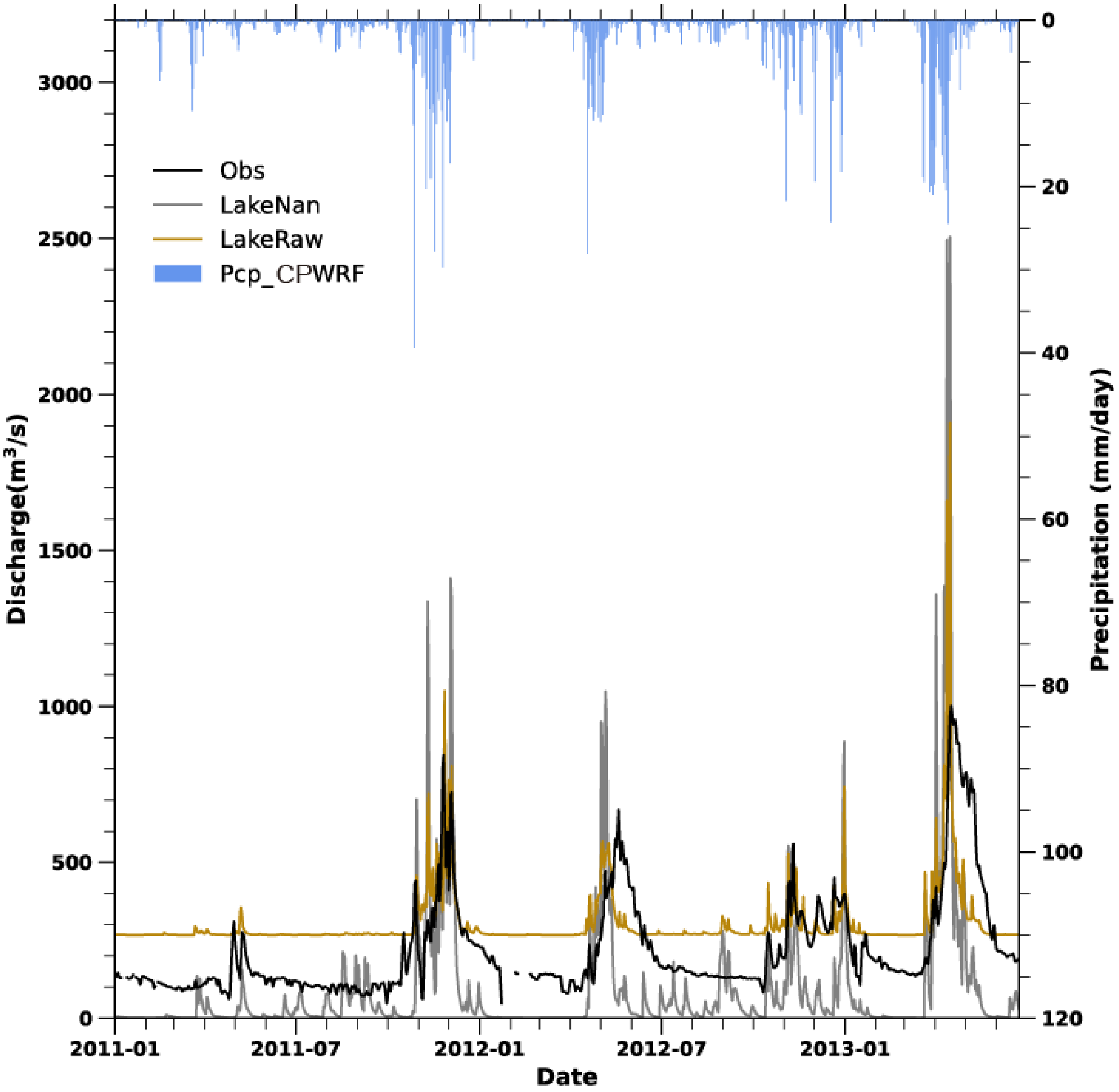

Figure 4. The simulated daily discharges from WRF-Hydro modeling without the lake/reservoir module (LakeNan, the grey line) and that with the lake/reservoir module using parameters from the LakeNan (LakeRaw, the brown line) against the observations (the black line), as well as the daily precipitation from convection-permitting CPWRF simulation (Pcp_CPWRF, the blue bar).

4.2.2. Spin-up time

In the LakeRaw simulation, the spin-up sensitivity is highlighted by the discharge during 2011-2014 from the 17 spin-up experiments (Fig. 5 and Table 3). The simulated discharge at the Garissa station, on the first day (26 November 2011, the observed Peak-Flow day), differs between almost every experiment. The simulated Peak-Flow at the Garissa station decreases as the spin-up time gets shorter, which reaches 485 $m^3 s^{-1}$ in the 12-year spin-up experiment (12y spin-up in Fig. 5a) but only 211 $m^3 s^{-1}$ in the 1-day spin-up experiment (1d spin-up) from the LakeRaw simulation. The reduction of first-day discharge suggested that insufficient spin-up time results in more runoffs being allocated to soil moisture and groundwater, which have not yet reached equilibrium. In general, Peak-Flow runoff increases slightly with longer spin-up times, up to the 6-year spin-up (Fig. 5 b). Also, the average discharge shows distinct sensitivity to different spin-up times (Figs. 5 d-e). The average discharge at Garissa over the entire period, as well as during the rainy and dry seasons from 2011-2014, shifted from an underestimation of -49%, -44%, and -52% in the 1-day spin-up experiment to an overestimation of 21%, 54%, and 7% in the 12-year spin-up experiment. The LakeRaw simulation generally needs approximately four years for the annual discharge at Garissa to stabilize (Figs. 5d-e).

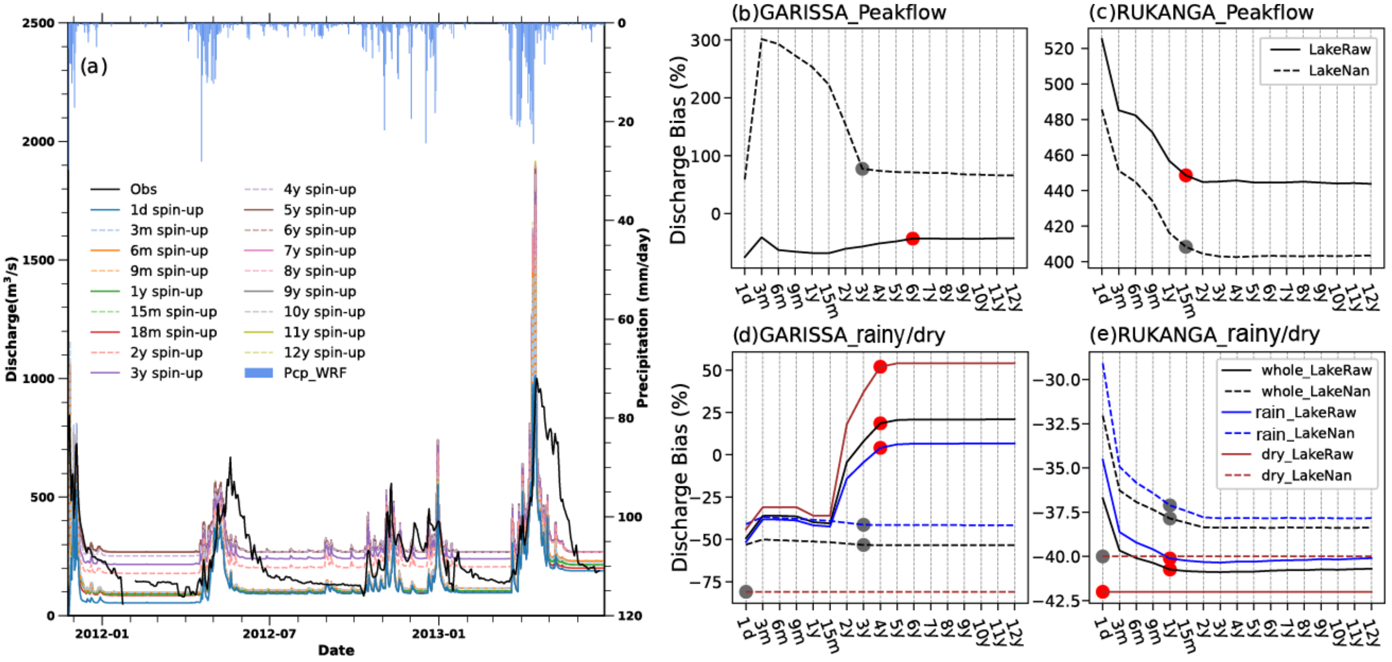

Figure 5. Sensitivity analysis results from 17 different spin-up experiments. (a) displays the simulated discharge with spin-ups (the colored lines) ranging from 1 day (1d spin-up) to 12 years (12y spin-up), against the observations (Obs, the black line) for the LakeRaw module. The blue bars indicate the daily precipitation from convection-permitting WRF simulation. (b-e) donates the model-data bias of discharge at Garissa (b and d), Rukanga (c and e) with the increase of spin-up time, which is from LakeNan (WRF-Hydro simulation with lake/reservoir module, solid line) or LakeRaw (WRF-Hydro simulation without lake/reservoir module using parameters from LakeNan, dashed line) over the entire year (black line), rainy season (March-May and October-December, blue line) and dry season (January-February and June-September, red line). The dot indicates the spin-up time required for LakeRaw (red) or LakeNan (grey) to reach equilibrium. Therein, Peak-Flow (Peakflow) is the largest daily discharge over the 21 days centered around the observed peak (largest observed daily discharge over 2011-2014).

The initial time differs spatially, with shorter spin-up in the upstream area compared to the downstream. In the LakeNan simulation, the initialization time of discharge metrics (i.e. Peak-Flow, average discharge, rainy season flow, and dry season flow) at Rukanga station upstream is less than 2 years, while at the downstream Garissa, it can extend to 3 years. The longer spin-up in the downstream area might be ascribed to the larger drainage area which requires a longer convergence time compared to the upstream. The prolongation of spin-up time is more distinct in the simulation with lake/reservoir module than in the one without it. In the LakeRaw simulation, the initialization time for discharge metrics at the upstream (Rukanga station) remains under 2 years, while the initialization time for Peak-Flow at the downstream (Garissa station) extends to 6 years. This significant prolongation of spin-up time indicates the lake/reservoir affection.

Lake/reservoir module seems to prolong the required spin-up time for the downstream area (Fig. 5b). In addition to the Peak-Flow, the spin-up time for the whole period, dry season and rainy season flow is prolonged to 4 years in the LakeRaw simulation, compared to the 3, 0 and 3 years, respectively, in the LakeNan simulation. The larger spin-up difference in dry season discharges between the LakeRaw (3 years) and LakeNan (0 years) simulations demonstrates a greater sensitivity of dry season to the lake/reservoir module, compared to the rainy season.

The water levels from the lake/reservoir-integrated model show a consistent spin-up period of 4 years across nearly all five lakes for the entire period, as well as during both the rainy and dry seasons (Fig. S2). Although KIAMBERE (one of the five lakes) exhibits a spin-up period of 3 years during the rainy season (Fig. S2 e), it can be considered nearly 4 years due to the uncertainty in determining the spin-up time required for the stabilization of specific variables. Since the lakes are interconnected, the stabilization time is governed by the longest spin-up period. This may result in nearly the same initialization time for all five lakes (Table 1).

4.2.3. Sensitivity analysis from hydrological parameters

The MannN parameter exhibits a substantial impact on the peak flow, with lower values corresponding to higher discharge peaks (Fig. 6 a and Table S3). As the MannN scale decreases from 4 to 0.1, the average discharge at Garissa increases from 294 m^3 s^{-1} to 297 m^3 s^{-1} and Peak-Flow increases from 975 m^3 s^{-1} to 1309 m^3 s^{-1}. In addition, the smaller MannN value delays the arrival of peak flows, shifting the Peak-Flow date from 6 December 2011 to 2 December 2011—an advance of four days—as MannN decreases from 4 to 0.1. This effect is due to MannN representing channel roughness, which influences both streamflow transit time and volume.

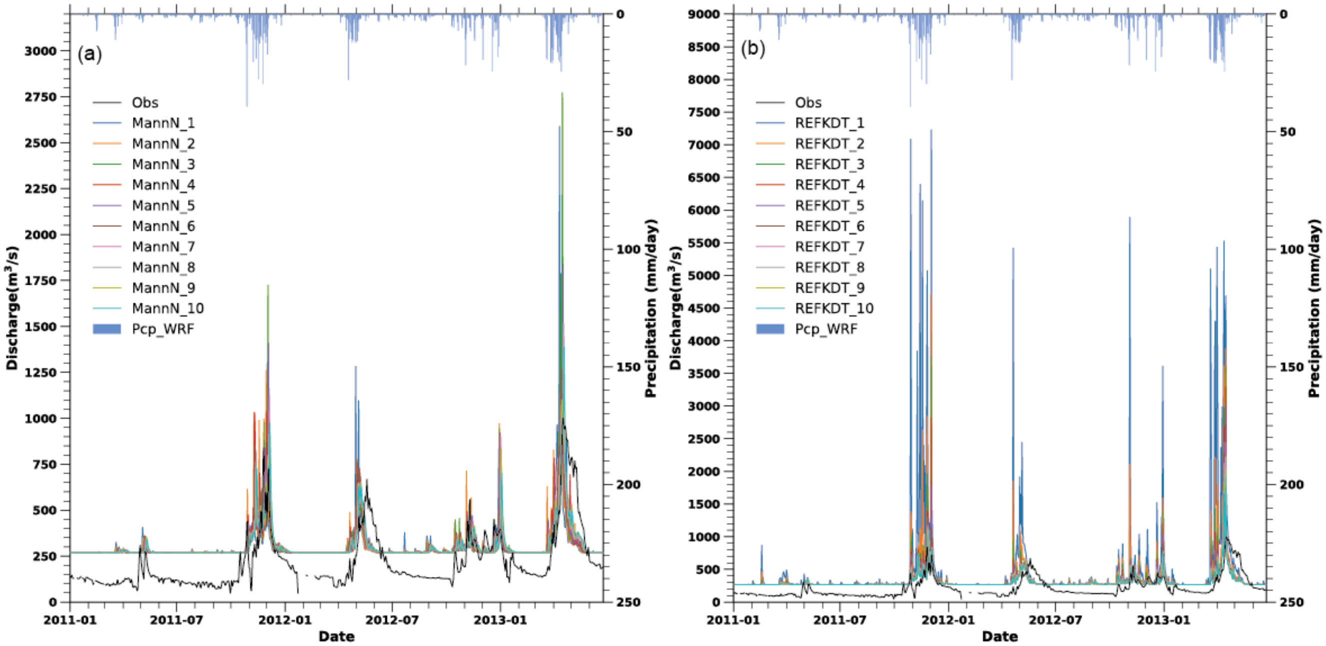

Figure 6. The simulated WRF-Hydro discharge at Garissa from January 2011 to June 2013 from Manning roughness parameter (MannN) and runoff infiltration coefficients (REFKDT) sensitivity tests, against the observation (Obs). MannN (or REFKDT) test consists of ten simulations, with the MannN (or REFKDT) ranging from a near-zero (or 0.02) scale in MannN_1 (or REFKDT_1) experiment to a scale of 4 (or 1) in MannN_10 (or REFKDT_10) with nearly equal intervals in between. Precipitation from the WRF simulation (Pcp_CPWRF) is shown at the top.

Similarly, the REFKDT parameter also significantly impacts peak discharge in response to heavy rain. An increase in REFKDT generally results in decreased discharge (Fig. 6 b and Table S4). Specifically, when the REFKDT scaling factor changes from 0.02 (REFKDT equals 0.1) to 1 (REFKDT equals 5), the Peak-Flow decreases from 7229 m^3 s^{-1} to 1092 m^3 s^{-1}. In the WRF-Hydro modeling system, the REFKDT parameter governs surface infiltration by partitioning runoff into the surface and subsurface components (Schaake et al., 1996). A higher REFKDT value allows more water into the subsurface, thereby reducing surface runoff and peak discharge.

However, both MannN and REFKDT have minimal effects on alleviating the underestimation of dry season flow shown in the above WRF-Hydro simulations with the lake/reservoir module (LakeRaw) (Fig. 4). The dry season flow remains largely unchanged despite variations in these two parameters.

4.2.4. Sensitivity analysis from groundwater components

Overall, adjusting groundwater component options could slightly alleviate the overestimation of dry season flow (Fig. 7 and Table S5). The dry season flows from the two experiments remain large overestimations with a considerable bias of 122 (81 %) and 161

(107 %) m^{3} s^{-1}, respectively. However, in the GWBASESWCRT_Passthrough experiment, the simulated discharge fluctuation aligns better with the observation, compared to the GWBASESWCRT_Sink experiment. The determination coefficients (r^{2}) of the simulated discharge against the observation are 0.56 and 0.33 in the GWBASESWCRT_Passthrough and GWBASESWCRT_Sink experiments, respectively. Besides, the discrepancies in the waveform in the GWBASESWCRT_Sink experiment cause an earlier prediction of flood retreat. Given the relatively better performance of the GWBASESWCRT_Passthrough experiment, we selected the pass-through bucket module for the subsequent sensitivity analysis and calibration experiment.

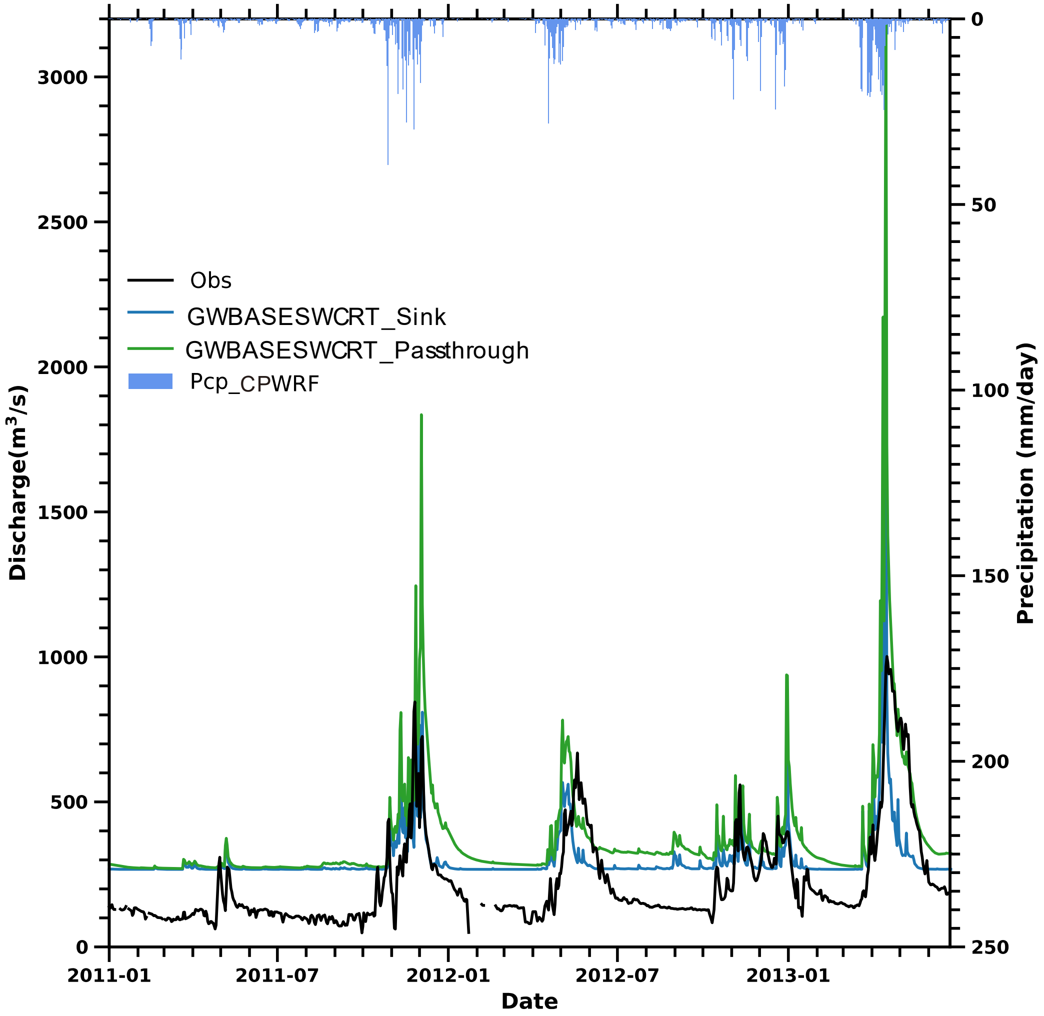

Figure 7. The discharge evolution of the two experiments and the observation. One experiment creates a sink at the bottom of the soil column, where water drains out of the system (GWBASESWCRT_Sink), while the other bypasses the bucket model and directly transfers all flow from the bottom of the soil column into the channel (GWBASESWCRT_Passthrough). Precipitation from the CPWRF simulation (Pcp_CPWRF) is shown at the top.

4.2.5. Sensitivity analysis from lake/reservoir-related parameters

From the results of Morris method (Fig. 8 and Table S6), lake/reservoir-related parameters (i.e., LkMxE, WeirE, WeirC WeirL, OrificeA，OrificeC, and OrificeE) show a clear influence on the discharge at Garissa. The overestimation of discharge was reduced in the best-performing simulation with the largest NSE (represented by the red line in Fig. 8 a). Among the eight lake/reservoir-related parameters, WeirE is the most sensitive, as indicated by its top sensitivity ranking (Fig. 8 b). Modifying the WeirE from its maximum (maximum water level plus half water depth) to its minimum (the default Orifice elevation) in the LakeRaw model with other parameters set at their defaults (Table S6), resulted in the average discharge varying from 311 m^{3} s^{-1} to 38 m^{3} s^{-1}, with the model-data bias from 19 % to less than -85 %. This sensitivity is particularly pronounced during the dry season, with a bias difference of 244 m^3 s^{-1} on average during 2011-2014, corresponding to -163 % of the observed values. This finding highlights that adjusting lake/reservoir-related parameters can significantly reduce the overestimation of dry season flow, showing promise for improving the model's overall performance. Notably, the eight parameters exhibit distinct interdependence, as indicated by the large value of sigma/u (> 0.5) (Fig. 8 c), suggesting that parameter optimization should be conducted globally rather than locally.

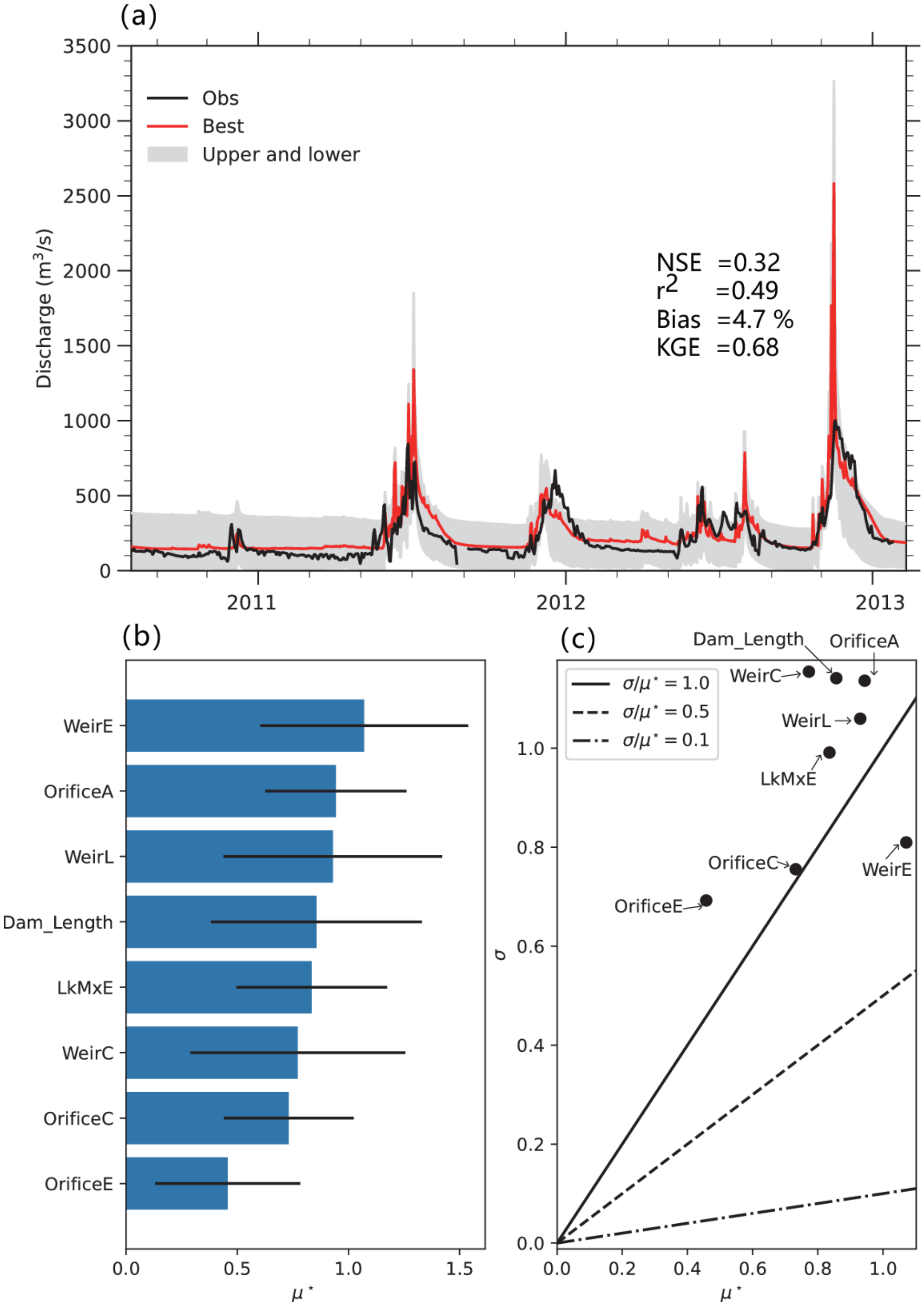

Figure 8. The Morris results, including simulated discharge from 90 experiments against the observation (a), the sensitivity ranking of parameters (b), and their interdependence (c). Nash-Sutcliffe Efficiency (NSE), coefficient of determination (r^2), bias (Bias, unit: %), and Kling-Gupta Efficiency (KGE) are calculated based on the best-simulated discharge at Garissa (shown in the red line, which corresponds to the largest NSE) against the observations. The u* donates the sensitivity of a given parameter, with a higher value indicating greater sensitivity. The large value of σ/u* indicates stronger dependencies with other parameters.

Although adjusting lake/reservoir-related parameters can alleviate the overestimation of dry season flow, it induces a new issue: a simultaneous decrease in rainy season discharge, leading to its underestimation. Modifying WeirE in the LakeRaw model (keeping other parameters at their default settings), results in a shift of rainy season flow from a wet bias (52 m^3 s^{-1}, 19 %) to a dry bias (-197 m^3 s^{-1}, -71 %). This bias change is also observed in the Peak-Flow, which varied from an overestimation of 165 m^3 s^{-1} (20 %) to an underestimation of -127 m^3 s^{-1} (-16 %). Fortunately, the rainy season flow underestimation could be re-adjusted by REFKDT or MannN, as well as the Peak-Flow.

Lakes with larger surface areas appear to play a dominant role in affecting discharge biases, as shown in Fig. S4. Adjusting parameters of larger lakes, such as MASINGA, KAMBURU, and KIAMBERE, leads to greater variations, reflected in larger standard deviations, compared to smaller lakes like GITARU and KINDARUMA. Among the five lakes, MASINGA (the largest, with an area of 111.6 km²) exhibits the most significant impact on discharge, with standard deviations of 21 % for Peak-Flow, 23.7 % for average discharge, 19 % for rainy season flow, and 34 % for dry season flow. In contrast, KINDARUMA (the smallest with an area of 2.1 km²) exhibits the least impact on discharge, with near-zero standard deviations (0.1 %, 0.3 %, 0.2 %, and 0.6 %, respectively).

4.2.6. The optimized results of WRF-Hydro modeling with lake/reservoir module

Based on the sensitivity analysis result, we conducted a calibration involving the parameters outlined above, and the results are shown in Fig. 9 and Table S2. Calibration of the WRF-hydro modeling system with lake/reservoir module greatly improves the simulation of river discharges in the TRB. The simulated discharge from LakeCal with an NSE of 0.57 and a bias of 9 %, is more consistent with the observed flow process, compared to LakeRaw with an NSE of 0.01 and a bias of 40 %. The significant overestimation of discharge in the LakeRaw (Sect. 4.2.1) model was notably reduced through the calibration of the lake/reservoir module, although a slight overestimation remains.

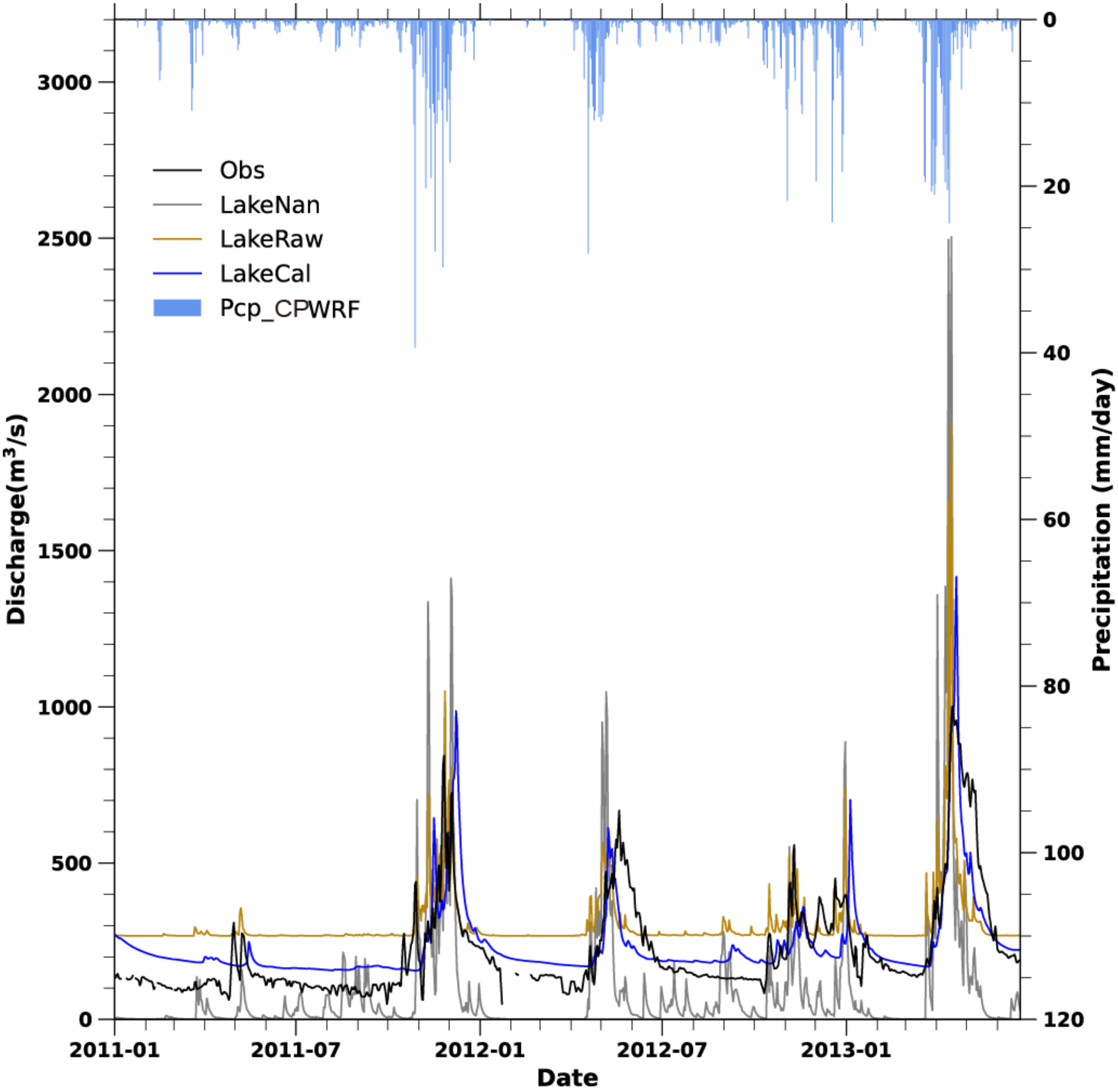

Figure 9. The simulated discharges from three WRF-Hydro simulations against the observation. The three include WRF-Hydro simulation without lake/reservoir module (LakeNan in grey), WRF-Hydro with lake/reservoir module based on parameters from the LakeNan (LakeRaw, in brown), and the well-calibrated WRF-Hydro with lake/reservoir module (LakeCal, in blue). Precipitation from the CPWRF simulation (Pcp_CPWRF) is shown at the top.

Notably, the modeling performance of WRF-Hydro simulation with the lake/reservoir module (LakeCal) is much better than that without lake/reservoir module (LakeNan). The NSE and bias are -1.09 and -53 % in LakeNan simulation, compared to 0.57 and 9 % in LakeCal simulation. The improvement is particularly evident during dry season flow and Peak-Flow simulation, despite a slight overestimation of dry season flow. The calibration of the WRF-Hydro modeling system with lake/reservoir module corrects the overestimation of dry season flow by 71 m^3 s^{-1}, reducing the dry season flow from 271 m^3 s^{-1}(with a bias of 81 %) to 200.1 m^3 s^{-1} (with a bias of 34 %). Besides, the deviation in Peak-Flow, indicated by a bias of 174 % (144 m^3 s^{-1}) decreased in LakeCal to a bias of 24 % (206 m^3 s^{-1}) in LakeRaw. Consistently, the overestimation of averaged discharge in the rainy season flow was reduced, with the bias changing from 22 % to -2 %. Due to this improvement in dry season flow, Peak-Flow simulation and rainy season flow, LakeCal better captures seasonal variation than the other two models. The r^2 is 0.75 in the LakeCal model, calculated over the simulated monthly discharge against the observation, compared to 0.66 in the LakeNan simulation. Furthermore, the LakeCal could better capture the hydrograph shape during the rise and recession of floods, as indicated by the improved r^2 of 0.59, compared to 0.30 in the LakeNan and 0.33 in the LakeRaw. For example, during the MAM period in 2012 and 2013, the simulated onset and recession times of flooding by LakeCal were closer to the observed, than those from the LakeRaw and LakeNan. The earlier estimation of flood onset times in the LakeRaw was significantly alleviated in the LakeCal. The better fit of the simulated discharge against the observation during flood rising and falling times in the WRF-Hydro system with lake/reservoir module indicates a promising ability to accurately forecast floods.

5. Discussion

5.1. Attribution of hydrological simulation enhancement

The above skilled WRF-Hydro simulation of LakeCal (Fig. 9) could be attributed to the integration of CPWRF simulation and the inclusion of lake/reservoir module. To quantitively assess the contributions from CPWRF simulation and lake/reservoir module to discharge performance, we compared three models (LakeNan, LakeCal, and LakeCal-ERA5) and the results are presented in Figs. 9-10 and Table S2.

The well-calibrated lake/reservoir-integrated model forced by CPWRF output (LakeCal), outperforms both no-lake/reservoir model driven by CPWRF output (LakeNan) and lake/reservoir-integrated model forced by ERA5 (LakeCal-ERA5). Comparing LakeCal to LakeCal-ERA5, the refined precipitation from CPWRF notably enhances the WRF-Hydro modeling performance, particularly in reducing the peak false simulation (Fig. 10 a). The simulation skill indicated by NSE, rises from 0.04 (LakeCal-ERA5) to 0.57 (the LakeCal) (Table S2), resulting in an NSE increase of 0.53. Comparing the LakeCal to LakeNan, the inclusion of the lake/reservoir module significantly improves the WRF-Hydro performance, distinct in alleviating the underestimation of the dry season flow and the overestimation of the peak flow. The NSE rises from -1.10 (LakeNan) to 0.57 (LakeCal), leading to an NSE increase of 1.67. Dividing the total increases of NSE, improvements in hydrological simulation could be attributed 24 % (an NSE increase of 0.53) to the precipitation simulated by CPWRF and 76 % (an NSE increase of 1.67) to the inclusion of the lake/reservoir module.

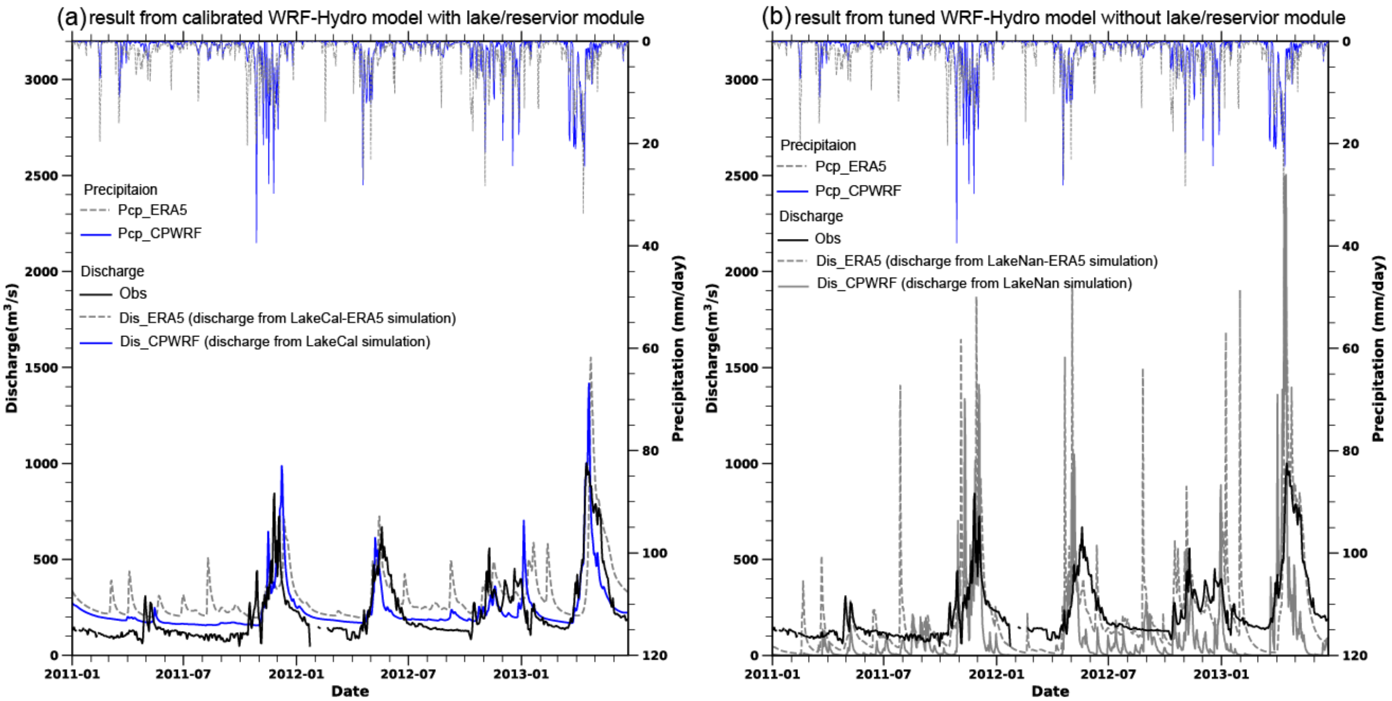

Figure 10. The precipitations from CPWRF (Pcp_CPWRF, solid line on the top) and ERA5 (Pcp_ERA5, dash line on the top), as well as the simulated daily discharge evolution from WRF-Hydro driven by CPWRF precipitation (Dis_CPWRF, solid line at the bottom colored blue in a and grey in b) and ERA5-precipitation (Dis_ERA5, dashed line at the bottom in both a and b) against the observation (black dashed line). (a) and (b) indicate the results from the calibrated WRF-Hydro model with and without the lake/reservoir model, respectively. LakeCal-ERA5 or LakeCal indicates well-calibrated lake/reservoir-integrated WRF-Hydro simulation driven by ERA5 data or CPWRF output, while LakeNan-ERA5 or LakeNan indicates WRF-Hydro simulation without lake/reservoir module driven by ERA5 data or CPWRF output.

5.2. Hydrological modeling improvement from CPWRF precipitation

Dynamic downscaling at convection-permitting resolution allows for a more accurate representation of precipitation processes. The CPWRF simulation enhances local (e.g., mesoscale) processes and interactions between local and large-scales, especially over complex terrain (Kendon et al., 2021; Guevara Luna et al., 2020; Schmidli et al., 2006; Schumacher et al., 2020; Li et al., 2020). As a result, CPWRF potentially contributes to improving precipitation simulation in our study (Sect. 4.1), especially reducing bias in seasonal precipitation over mountainous areas, and light rainfall (1-15mm day^{-1}) probability in the dry season compared to ERA5 (Fig. 3 and Table 8).

The improvement in the seasonal precipitation over mountainous regions and rainfall probability can be supported by the spatial distribution of the added value (AV) in seasonal precipitation with respect to the driving forces (Fig. S2). The CPWRF simulation adds consistent value to ERA5 over the mountainous areas across all four seasons (MAM, OND, JF, and JJAS). The area with positive AV is mainly over Mount Kenya and its surrounding areas, with the positive AV being particularly distinct during the dry season. CPWRF also adds value to ERA5 in the light rainfall probability (Fig. S2 f-k), as demonstrated in Sect. 4.1. The basin averaged AV of CPWRF over the probability of light precipitation events are 0.32, 0.26, 0.30, and 0.07 in MAM, OND, JF, and JJAS, respectively. The positive AV of CPWRF with respect to ERA5 over the extreme rainfall probability, also concentrates around Mount Kenya, consistently across all four seasons (Fig. S2 l-p). Previous studies (Giorgi et al., 2022) have demonstrated that the added value of CPWRF simulations is influenced by various factors, including timescale, variables, regions, and uncertainty of the benchmark. Therefore, further in-depth research is required for a more reliable AV assessment.

Due to the precipitation improvement from WRF, hydrological simulation with CPWRF precipitation as a driving force (LakeCal), showed significant improvements, compared to simulations driven by ERA5 (LakeCal-ERA5) (Fig. 10a). These improvements are particularly notable in reducing false peak simulations, likely due to the reduction in the overestimation of light rainfall probability. The enhancement in peak flow simulation is also observed in the WRF-Hydro model without the lake/reservoir module (Fig. 10b).

5.3. Hydrological modeling improvement from lake/reservoir module

The lake/reservoir module is crucial for improving hydrological simulations over TRB in East Africa. Several factors could contribute to overestimation issues presented in the LakeRaw simulation, even with adequate spin-up time, such as the groundwater component, key hydrological parameters, and lake/reservoir-related parameters. Despite some adjustments, the groundwater component (Sect. 4.2.4) and key hydrological parameters (Sect. 4.2.3) have a limited ability to alleviate the overestimation of dry season flow in lake/reservoir-integrated WRF-Hydro simulation without calibration (LakeRaw). In contrast, tuning lake/reservoir-related parameters could significantly influence downstream discharge (Sect. 4.2.6). This underscores the critical role of the lake/reservoir module in enhancing hydrological simulations in the data scarcity regions that contain lakes or reservoirs.

Lakes/reservoirs play a crucial regulatory role, storing water during the rainy season (especially the peak flow period) and releasing water during the dry season (Zajac et al., 2017; Hanasaki et al., 2006). In our study, hydrological simulations without lake/reservoir module (LakeNan) in the TRB, which includes five lakes, show significant underestimation (-78 %) in dry season flow and overestimation (24 %) in Peak-Flow. The underestimation of dry season flow and overestimation of Peak-Flow are well-documented issues in East Africa, as noted by Arnault et al. (2023). Previous studies demonstrated that enhancing reservoir hydrological processes can improve simulation accuracy (Hanasaki et al., 2006; Lehner et al., 2011) for basins with reservoirs or lakes. Our results confirm that the well-calibrated lake/reservoir-integrated WRF-Hydro system significantly reduces the underestimation of dry season flow and overestimation of Peak-Flow. The lake/reservoir module helps to adjust the dry season flow bias from -78 % in LakeNan simulation to 34 % in the LakeCal, despite some remaining positive bias. The Peak-Flow bias in the lake/reservoir simulation decreased to 17 %, compared to the value 24 % in LakeNan simulation.

5.4. Uncertainties

Although CPWRF simulation shows improved skills evidently in seasonal precipitation around Mount Kenya and light rainfall probability during the dry season, it is notable that CPWRF still displays uncertainties. This uncertainty involves wet biases in rainy seasons and dry biases in dry seasons (Figs. 2, Table 7), as well as the overestimation of small rainfall (0-20mm/day) probability and the underestimation of extreme rainfall (> 20 mm/day) probability (Figs. 5 and Table 8). Although seasonal precipitation simulation from CPWRF exhibits an improvement in mountainous areas compared to ERA5, it is slightly degraded in the plain areas (Table S1). The uncertainty might come from the driving data ERA5, which could be observed with the same bias as the CPWRF result. Good quality forcing drivers could be further used to improve the precipitation simulation in future work. Besides, the benchmark (IMERG) in the data-scarce area presents challenges for precipitation evaluation. The uncertainty from IMERG precipitation over East Africa (Dezfuli et al., 2017), may complicate precipitation evaluation. In our study, CPWRF simulation shows an underestimation of extreme precipitation (i.e. 90-100 quantiles) against the IMERG (Fig. 5 b and f), while the simulated discharge from LakeCal, driven by CPWRF precipitation, does not exhibit the expected underestimation of extreme flow when compared to observations (Fig. 10b). The absence of the underestimation of extreme flow suggests IMERG may overestimate extreme precipitation compared to its actual representation. The overestimation of IMERG precipitation in Africa has been demonstrated in previous research (Maranan et al., 2020; Dezfuli et al., 2017), which could create the illusion of underestimation from WRF. Such erroneous underestimation of extreme precipitation from CPWRF was also indicated by the general overestimation of extreme flow in LakeCal simulation (Fig. 10 a-b). Therefore, we believe that the potential advantages of the CPWRF simulation are likely greater than what we have demonstrated by our result. Future work could benefit from incorporating more reliable observational data to enhance precipitation evaluation.

Different metrics (r, bias, and normalized standardized deviation) were used to provide a more comprehensive assessment of the CPWRF's performance, which may cause contradictory or different evaluations of its skill. Each metric emphasizes different aspects of model performance and leads to divergent conclusions about the model's strengths or weaknesses. For instance, seasonal precipitation from the CPWRF result exhibits apparent added value to the forcing data over mountainous areas (Fig. S2 a-e), which however is not distinct in the Taylor figure (Fig. S1). This discrepancy arises because the region with apparent added value is mainly centered on Mount Kenya, whereas the mountainous region in the Taylor diagram analysis includes areas above 1600 m, extending beyond Mount Kenya. Therefore, further in-depth research is needed to fully assess the performance of CPWRF with these different metrics and explain the possible discrepancy.

Also, uncertainty may exist in the sensitivity analysis of the simulated peak flow to spin-up time, which was based on a single event (the largest observed peak from 2010 to 2014) at a specific discharge station (i.e., Garissa or Rukanga). The conclusion, especially about the spin-up time required for model stabilization, may vary when different regions or other peak flow events are considered. For example, a WRF/WRF-Hydro simulation (Lu et al., 2020) exhibits that initialization times needed for soil moisture stabilization differ for different basins in Western Norway. The varying spin-up periods required for flow stabilization between the dry and rainy seasons (Sect. 4.2.2 and Fig. 5 d-e) indicate the possible sensitivity of peak flow to spin-up duration across different peak flow events. The sensitivity of different regions and other peak flow events to spin-up time will be further investigated.

Additionally, the hydrological model needs to be perfected although the lake/reservoir module improves WRF-Hydro simulation. The lake/reservoir module, expressed as a water balance equation with a simple level-pool scheme, could induce uncertainties in the hydrological simulation, due to the insufficient physical mechanism, and lack of consideration for human activities and small tributaries in the upstream of lakes. For example, it shows a limited skill in simulating water levels (Fig. S5 and Table S6). In the LakeCal simulation, the water level deviation can reach -191 m (-28 % of the observation averaged over 2011-2015) at KIAMBERE. Moreover, the water level fluctuations between the simulation and observation show large differences, with r^2 of the simulated water level against the observation less than 0.25 for the five lakes. The groundwater component can also cause uncertainties, as we used a pass-through bucket module that transfers all flow from the soil column into the channel without recharging groundwater. This approach might not present the intermittent groundwater recharge from seasonal rainfall in the TRB (Taylor et al., 2013). This leads to potential inaccuracies in simulating groundwater processes and their interaction with surface water in East Africa. Future work will focus on refining the hydrological simulation over East Africa with an advanced dynamical lake/reservoir module (Wang et al., 2019) and an enhanced groundwater component.

6. Conclusion

In this study, we conducted a seamless and consistent meteorological-hydrological modeling system to improve hydrological simulation in East Africa, demonstrated through a case study in Tana River Basin (TRB). The main findings are as follows.

(1) The refined precipitation from CPWRF simulation significantly improves the hydrological performance. Compared to ERA5-driven simulation (LakeCal-ERA5), the CPWRF-driven WRF-Hydro simulation (LakeCal) increases NSE by 0.53, contributing to a 24 % improvement in the hydrological simulation. CPWRF outperforms ERA5, by reducing bias in seasonal precipitation mainly over Mount Kenya region and in light rainfall (1-15 mm day^{-1}) during the dry season. The CRWRF-driven LakeCal simulation effectively reduced peak false occurrences, compared to ERA5-driven results (Lake-ERA5).

(2) Integrating the lake/reservoir module in the WRF-Hydro system reduces bias in dry season flow and peak flow, achieving an NSE improvement of 1.67 (from -1.10 to 0.57), contributing to a 76 % improvement in hydrological simulation, compared to that without the lake/reservoir module (LakeNan). The lake-integrated model significantly affects discharge through lake/reservoir-related parameters and increases the sensitivity of discharge to spin-up time, particularly during the dry season flow. However, adjustments to key parameters, such as runoff infiltration rates, Manning's roughness coefficient, and groundwater components, have minimal impact on the dry season flows.

Our study highlights the improved streamflow simulations achieved by integrating a lake/reservoir module with CPWRF outputs in the WRF-Hydro modeling system, offering a robust tool for hydrological modelling in data-scarce regions like East Africa. This advancement lays the foundation for more accurate flood and drought predictions, facilitating informed water resource management, risk mitigation, and sustainable environmental stewardship in regions vulnerable to hydrological variability and change.

Acknowledgments

This research was supported by the National Natural Science Foundation of China (Grants 42205057), the European Union's Horizon 2020 research and innovation program under grant agreement no. 869730 (CONFER), the National Natural Science Foundation of China (Grants 42125502 and 42371367), Project funded by China Postdoctoral Science Foundation (Grant 1232192), the German Science Foundation (DFG) project: Large-Scale and High-Resolution Mapping of Soil Moisture on Field and Catchment Scales Boosted by Cosmic-Ray Neutrons (COSMIC-SENSE, FOR 2694, grant KU 2090/12-2). The co-author Pratik has been supported by the Research Council of Norway (project number 326122). The computer resources were available through the RCN's program for supercomputing (NOTUR/NORSTORE), projects NN9853K and NS9853K. Thanks to ChatGPT for improving the language.

Code availability

WRF code is available from https://github.com/wrf-model/WRF. WRF-Hydro code is available from https://github.com/NCAR/wrf_hydro_nwm_public.

Data availability

All WRF-Hydro simulation data in this paper are available from the authors upon request (lingzhang@cug.edu.cn and luli@norceresearch.no).

Competing interests

The authors declare that they have no conflict of interest.

Author contribution

Ling Zhang and Lu Li jointly developed and designed the sensitivity experiments. Ling Zhang further refined the idea and experiment, conducted the WRF-Hydro model runs, performed the data analysis, and conducted the visualization. Ling Zhang, Lu Li, and Zhongshi Zhang contributed to the original manuscript and handled subsequent revisions. Joël Arnault conducted the convection-permitting WRF simulations and, together with Lu Li and Anthony Musili Mwanthi, designed and set up the WRF-Hydro modeling with lake/reservoir module at TRB. Zhongshi Zhang, Xiaoling Chen, Jianzhong Lu, Joël Arnault, Stefan Sobolowski, Pratik Kad, and Zhengkang Zuo contributed to the review & editing. Mohammed Abdullahi Hassan collected and provided the observation discharge data and offered suggestions for flood simulation improvements. Tanja Portele and Harald Kunstmann contributed to the WRF simulations and uncertainty discussion.

References

Adjei, K. A., Ren, L., Appiah-Adjei, E. K., and Odai, S. N.: Application of satellite-derived rainfall for hydrological modelling in the data-scarce Black Volta trans-boundary basin, Hydrology Research, 46, 777–791, https://doi.org/10.2166/nh.2014.111, 2015.

Ajami, H., McCabe, M. F., Evans, J. P., and Stisen, S.: Assessing the impact of model spin-up on surface water-groundwater interactions using an integrated hydrologic model, Water Resources Research, 50, 2636–2656, https://doi.org/10.1002/2013WR014258, 2014a.

Ajami, H., Evans, J. P., McCabe, M. F., and Stisen, S.: Technical note: Reducing the spin-up time of integrated surface water-groundwater models, Hydrology and Earth System Sciences, 18, 5169–5179, https://doi.org/10.5194/hess-18-5169-2014, 2014b.

Alavoine, M. and Grenier, P.: The distinct problems of physical inconsistency and of multivariate bias involved in the statistical adjustment of climate simulations, International Journal of Climatology, 43, 1211–1233, https://doi.org/10.1002/joc.7878, 2023.

Anyah, R. O. and Semazzi, F. H. M.: Climate variability over the Greater Horn of Africa based on NCAR AGCM ensemble, Theoretical and Applied Climatology, 86, 39–62, https://doi.org/10.1007/s00704-005-0203-7, 2006.

Arnault, J., Mwanthi, A. M., Portele, T., Li, L., Rummler, T., Fersch, B., Hassan, M. A., Bahaga, T. K., Zhang, Z., Mortey, E. M., Achugbu, I. C., Moutahir, H., Sy, S., Wei, J., Laux, P., Sobolowski, S., and Kunstmann, H.: Regional water cycle sensitivity to afforestation: synthetic numerical experiments for tropical Africa, Frontiers in Climate, 5, https://doi.org/10.3389/fclim.2023.1233536, 2023.

Berthou, S., Rowell, D. P., Kendon, E. J., Roberts, M. J., Stratton, R. A., Crook, J. A., and Wilcox, C.: Improved climatological precipitation characteristics over West Africa at convection-permitting scales, Climate Dynamics, 53, 1991–2011, https://doi.org/10.1007/s00382-019-04759-4, 2019.

Biskop, S., Krause, P., Helmschrot, J., Fink, M., and Flügel, W. A.: Assessment of data uncertainty and plausibility over the Nam Co Region, Tibet, Advances in Geosciences, 31, 57–65, https://doi.org/10.5194/adgeo-31-57-2012, 2012.

Bitew, M. M. and Gebremichael, M.: Evaluation of satellite rainfall products through hydrologic simulation in a fully distributed hydrologic model, Water Resources Research, 47, https://doi.org/10.1029/2010WR009917, 2011.

Bonekamp, P. N. J., Collier, E., and Immerzeel, W.: The Impact of spatial resolution, land use, and spinup time on resolving spatial precipitation patterns in the Himalayas, Journal of Hydrometeorology, 19, 1565–1581, https://doi.org/10.1175/JHM-D-17-0212.1, 2018.

Chen, J., Brissette, F. P., and Leconte, R.: Uncertainty of downscaling method in quantifying the impact of climate change on hydrology, Journal of Hydrology, 401, 190–202, https://doi.org/10.1016/J.JHYDROL.2011.02.020, 2011.

Cosgrove, B. A., Lohmann, D., Mitchell, K. E., Houser, P. R., Wood, E. F., Schaake, J. C., Robock, A., Sheffield, J., Duan, Q., Luo, L., Higgins, R. W., Pinker, R. T., and Tarpley, J. D.: Land surface model spin-up behavior in the North American Land Data Assimilation System (NLDAS), Journal of Geophysical Research: Atmospheres, 108, https://doi.org/10.1029/2002jd003316, 2003.

Crook, J., Klein, C., Folwell, S., Taylor, C. M., Parker, D. J., Stratton, R., and Stein, T.: Assessment of the Representation of West African Storm Lifecycles in Convection-Permitting Simulations, Earth and Space Science, 6, 818–835, https://doi.org/10.1029/2018EA000491, 2019.

Dee, D. P., Uppala, S. M., Simmons, A. J., Berrisford, P., Poli, P., Kobayashi, S., Andrae, U., Balmaseda, M. A., Balsamo, G., Bauer, P., Bechtold, P., Beljaars, A. C. M., van de Berg, L., Bidlot, J., Bormann, N., Delsol, C., Dragani, R., Fuentes, M., Geer, A. J., Haimberger, L., Healy, S. B., Hersbach, H., Hólm, E. V., Isaksen, L., Kållberg, P., Köhler, M., Matricardi, M., Mcnally, A. P., Monge-Sanz, B. M., Morcrette, J. J., Park, B. K., Peubey, C., de Rosnay, P., Tavolato, C., Thépaut, J. N., and Vitart, F.: The ERA-Interim reanalysis: Configuration and performance of the data assimilation system, Quarterly Journal of the Royal Meteorological Society, 137, 553–597, https://doi.org/10.1002/qj.828, 2011.

Dezfuli, A. K., Ichoku, C. M., Huffman, G. J., Mohr, K. I., Selker, J. S., van de Giesen, N., Hochreutener, R., and Annor, F. O.: Validation of IMERG precipitation in Africa, Journal of Hydrometeorology, 18, 2817–2825, https://doi.org/10.1175/JHM-D-17-0139.1, 2017.

Dosio, A., Panitz, H. J., Schubert-Frisius, M., and Lüthi, D.: Dynamical downscaling of CMIP5 global circulation models over CORDEX-Africa with COSMO-CLM: evaluation over the present climate and analysis of the added value, Climate Dynamics, 44, 2637–2661, https://doi.org/10.1007/S00382-014-2262-X, 2015.

Folwell, S. S., Taylor, C. M., and Stratton, R. A.: Contrasting contributions of surface hydrological pathways in convection permitting and parameterised climate simulations over Africa and their feedbacks on the atmosphere, Climate Dynamics, 59, 633–648, https://doi.org/10.1007/s00382-022-06144-0, 2022.

Funk, C., Peterson, P., Landsfeld, M., Pedreros, D., Verdin, J., Shukla, S., Husak, G., Rowland, J., Harrison, L., Hoell, A., and Michaelsen, J.: The climate hazards infrared precipitation with stations - A new environmental record for monitoring extremes, Scientific Data, 2, https://doi.org/10.1038/sdata.2015.66, 2015.

Giorgi, F., Coppola, E., Jacob, D., Teichmann, C., Omar, S. A., Ashfaq, M., Ban, N., Bülow, K., Bukovsky, M., Buntemeyer, L., Cavazos, T., Ciarlo, J., da Rocha, R. P., Das, S., di Sante, F., Evans, J. P., Gao, X., Giuliani, G., Glazer, R. H., Hoffmann, P., Im, E. S., Langendijk, G., Lierhammer, L., Llopart, M., Mueller, S., Luna-Nino, R., Nogherotto, R., Pichelli, E., Raffaele, F., Reboita, M., Rechid, D., Remedio, A., Remke, T., Sawadogo, W., Sieck, K., Torres-Alavez, J. A., and Weber, T.: The CORDEX-CORE EXP-I Initiative: Description and Highlight Results from the Initial Analysis, Bulletin of the American Meteorological Society, 103, E293–E310, https://doi.org/10.1175/BAMS-D-21-0119.1, 2022.

Gochis, D. J., M. Barlage, A., Dugger, K., FitzGerald, L., Karsten, M., McAllister, J., McCreight, J., Mills, A., RefieeiNasab, L., Read, K., Sampson, D., and Yates, W. Y.: The WRF-Hydro modeling system technical description,(Version 5.0), 107 pp., 2018.

Guevara Luna, M. A., Casallas, A., Belalcázar Cerón, L. C., and Clappier, A.: Implementation and evaluation of WRF simulation over a city with complex terrain using Alos-Palsar 0.4 s topography, Environmental Science and Pollution Research, 27, 37818–37838, https://doi.org/10.1007/s11356-020-09824-8, 2020.

Hanasaki, N., Kanae, S., and Oki, T.: A reservoir operation scheme for global river routing models, Journal of Hydrology, 327, 22–41, https://doi.org/10.1016/j.jhydrol.2005.11.011, 2006.

Hersbach, H., Bell, B., Berrisford, P., Hirahara, S., Horányi, A., Muñoz-Sabater, J., Nicolas, J., Peubey, C., Radu, R., Schepers, D., Simmons, A., Soci, C., Abdalla, S., Abellan, X., Balsamo, G., Bechtold, P., Biavati, G., Bidlot, J., Bonavita, M., De Chiara, G., Dahlgren, P., Dee, D., Diamantakis, M., Dragani, R., Flemming, J., Forbes, R., Fuentes, M., Geer, A., Haimberger, L., Healy, S., Hogan, R. J., Hólm, E., Janisková, M., Keeley, S., Laloyaux, P., Lopez, P., Lupu, C., Radnoti, G., de Rosnay, P., Rozum, I., Vamborg, F., Villaume, S., and Thépaut, J. N.: The ERA5 global reanalysis, Quarterly Journal of the Royal Meteorological Society, 146, 1999–2049, https://doi.org/10.1002/qj.3803, 2020.

Huffman, G. J., Bolvin, D. T., Braithwaite, D., Hsu, K. L., Joyce, R. J., Kidd, C., Nelkin, E. J., Sorooshian, S., Stocker, E. F., Tan, J., Wolff, D. B., and Xie, P.: Integrated Multi-satellite Retrievals for the Global Precipitation Measurement (GPM) Mission (IMERG), Advances in Global Change Research, 67, 343–353, https://doi.org/10.1007/978-3-030-24568-9_19, 2020.

Ji, Z. and Kang, S.: Projection of snow cover changes over China under RCP scenarios, Climate Dynamics, 41, 589–600, https://doi.org/10.1007/s00382-012-1473-2, 2013.

Jimy Dudhia: Numerical Study of Convection Observed during the Winter Monsoon Experiment Using a Mesoscale Two-Dimensional Model, Journal of the Atmospheric Sciences, 46, 3077–3107, 1989.

Johnston, B. R., Xie, F., and Liu, C.: The Effects of Deep Convection on Regional Temperature Structure in the Tropical Upper Troposphere and Lower Stratosphere, Journal of Geophysical Research: Atmospheres, 123, 1585–1603, https://doi.org/10.1002/2017JD027120, 2018.

Julien, P. Y., Saghafian, B., and Ogden, F. L.: Raster-Based Hydrologic Modeling of Spatially-Varied Surface Runoff, JAWRA Journal of the American Water Resources Association, 31, 523–536, https://doi.org/10.1111/j.1752-1688.1995.tb04039.x, 1995.

Kad, P. and Ha, K. J.: Recent Tangible Natural Variability of Monsoonal Orographic Rainfall in the Eastern Himalayas, Journal of Geophysical Research: Atmospheres, 128, https://doi.org/10.1029/2023JD038759, 2023.

Kad, P., Ha, K. J., Lee, S. S., and Chu, J. E.: Projected Changes in Mountain Precipitation Under CO2-Induced Warmer Climate, Earth’s Future, 11, https://doi.org/10.1029/2023EF003886, 2023a.

Kawase, H., Hara, M., Yoshikane, T., Ishizaki, N. N., Uno, F., Hatsushika, H., and Kimura, F.: Altitude dependency of future snow cover changes over Central Japan evaluated by a regional climate model, Journal of Geophysical Research Atmospheres, 118, 12,444-12,457, https://doi.org/10.1002/2013JD020429, 2013.

Kendon, E. J., Prein, A. F., Senior, C. A., and Stirling, A.: Challenges and outlook for convection-permitting climate modelling, Philosophical Transactions of the Royal Society A: Mathematical, Physical and Engineering Sciences, 379, https://doi.org/10.1098/rsta.2019.0547, 2021.

Kerandi, N., Arnault, J., Laux, P., Wagner, S., Kitheka, J., and Kunstmann, H.: Joint atmospheric-terrestrial water balances for East Africa: a WRF-Hydro case study for the upper Tana River basin, Theoretical and Applied Climatology, 131, 1337–1355, https://doi.org/10.1007/s00704-017-2050-8, 2018.

Kerandi, N. M., Laux, P., Arnault, J., and Kunstmann, H.: Performance of the WRF model to simulate the seasonal and interannual variability of hydrometeorological variables in East Africa: a case study for the Tana River basin in Kenya, Theoretical and Applied Climatology, 130, 401–418, https://doi.org/10.1007/s00704-016-1890-y, 2017.

Kiptum, A., Antonarakis, A. S., Todd, M. C., and Guigma, K.: Characteristics, drivers, and predictability of flood events in the Tana River Basin, Kenya, Journal of Hydrology: Regional Studies, 53, https://doi.org/10.1016/j.ejrh.2024.101748, 2024.

Knoop, L., Sambalino, F., and van Steenbergen, F.: Securing water and land in the Tana basin: a resource book for water managers and practitioners., 2012.

Lange, K., Mogoi, S., and Weert, F. Van: IVM Institute for Environmental Studies The Economics of Ecosystem Services of the Tana River Basin, Wetlands Kenya, Technical Report, 1–2 pp., 2015.

Lehner, B., Liermann, C. R., Revenga, C., Vörömsmarty, C., Fekete, B., Crouzet, P., Döll, P., Endejan, M., Frenken, K., Magome, J., Nilsson, C., Robertson, J. C., Rödel, R., Sindorf, N., and Wisser, D.: High-resolution mapping of the world's reservoirs and dams for sustainable river-flow management, Frontiers in Ecology and the Environment, 9, 494–502, https://doi.org/10.1890/100125, 2011.

Li, C., Tang, G., and Hong, Y.: Cross-evaluation of ground-based, multi-satellite and reanalysis precipitation products: Applicability of the Triple Collocation method across Mainland China, Journal of Hydrology, 562, 71–83, https://doi.org/10.1016/j.jhydrol.2018.04.039, 2018.

Li, L., Gochis, D. J., Sobolowski, S., and Mesquita, M. D. S.: Evaluating the present annual water budget of a Himalayan headwater river basin using a high-resolution atmosphere-hydrology model, Journal of Geophysical Research, 122, 4786–4807, https://doi.org/10.1002/2016JD026279, 2017.

Li, L., Pontoppidan, M., Sobolowski, S., and Senatore, A.: The impact of initial conditions on convection-permitting simulations of a flood event over complex mountainous terrain, Hydrology and Earth System Sciences, 24, 771–791, https://doi.org/10.5194/hess-24-771-2020, 2020.

Lipzig, N. P. M. va., Walle, J. Van de, Belušić, D., Berthou, S., Coppola, E., Demuzere, M., Fink, A. H., Finney, D. L., Glazer, R., Ludwig, P., Marsham, J. H., Nikulin, G., Pinto, J. G., Rowell, D. P., Wu, M., and Thiery, W.: Representation of precipitation and top-of-atmosphere radiation in a multi-model convection-permitting ensemble for the Lake Victoria Basin (East-Africa), Climate Dynamics, 60, 4033–4054, https://doi.org/10.1007/s00382-022-06541-5, 2023.

Ma, Y., Yang, Y., Han, Z., Tang, G., Maguire, L., Chu, Z., and Hong, Y.: Comprehensive evaluation of Ensemble Multi-Satellite Precipitation Dataset using the Dynamic Bayesian Model Averaging scheme over the Tibetan plateau, Journal of Hydrology, 556, 634–644, https://doi.org/10.1016/j.jhydrol.2017.11.050, 2018.

Maingi, J. K. and Marsh, S. E.: Quantifying hydrologic impacts following dam construction along the Tana River, Kenya, Journal of Arid Environments, 50, 53–79, https://doi.org/10.1006/jare.2000.0860, 2002.

Maranan, M., Fink, A. H., Knippertz, P., Amekudzi, L. K., Atiah, W. A., and Stengel, M.: A process-based validation of gpm imerg and its sources using a mesoscale rain gauge network in the west african forest zone, Journal of Hydrometeorology, 21, 729–749, https://doi.org/10.1175/JHM-D-19-0257.1, 2020.

Mlawer, E. J., Taubman, S. J., Brown, P. D., Iacono, M. J., and Clough, S. A.: Radiative transfer for inhomogeneous atmospheres: RRTM, a validated correlated-k model for the longwave, Journal of Geophysical Research Atmospheres, 102, 16663–16682, https://doi.org/10.1029/97jd00237, 1997.

Monsieurs, E., Kirschbaum, D. B., Tan, J., Mateso, J. C. M., Jacobs, L., Plisnier, P. D., Thiery, W., Umutoni, A., Musoni, D., Bibentyo, T. M., Ganza, G. B., Mawe, G. I., Bagalwa, L., Kankurize, C., Michellier, C., Stanley, T., Kervyn, F., Kervyn, M., Demoulin, A., and Dewitte, O.: Evaluating TMPA rainfall over the sparsely gauged East African Rift, Journal of Hydrometeorology, 19, 1507–1528, https://doi.org/10.1175/JHM-D-18-0103.1, 2018.

Morris, M. D.: Factorial sampling plans for preliminary computational experiments, Technometrics, 33, 161–174, https://doi.org/10.1080/00401706.1991.10484804, 1991.

Naabil, E., Lamptey, B. L., Arnault, J., Kunstmann, H., and Olufayo, A.: Water resources management using the WRF-Hydro modelling system: Case-study of the Tono dam in West Africa, Journal of Hydrology: Regional Studies, 12, 196–209, https://doi.org/10.1016/j.ejrh.2017.05.010, 2017.

Nakanishi, M. and Niino, H.: An improved Mellor-Yamada Level-3 model: Its numerical stability and application to a regional prediction of advection fog, Boundary-Layer Meteorology, 119, 397–407, https://doi.org/10.1007/s10546-005-9030-8, 2006.

NASA: Deep Concern About Food Security in Eastern Africa, Nasa, 2022.

NASA: Devastating Flooding in East Africa, 2024.

Nash, J. E. and Sutcliffe, J. V: River flow forecasting through conceptual models part I--A discussion of principles, Journal of hydrology, 1970.

Nearing, G., Cohen, D., Dube, V., Gauch, M., Gilon, O., Harrigan, S., Hassidim, A., Klotz, D., Kratzert, F., Metzger, A., Nevo, S., Pappenberger, F., Prudhomme, C., Shalev, G., Shenzis, S., Tekalign, T. Y., Weitzner, D., and Matias, Y.: Global prediction of extreme floods in ungauged watersheds, Nature, 627, 559–563, 2024.

Oludhe, C., Sankarasubramanian, A., Sinha, T., Devineni, N., and Lall, U.: The role of multimodel climate forecasts in improving water and energy management over the tana river basin, Kenya, Journal of Applied Meteorology and Climatology, 52, 2460–2475, https://doi.org/10.1175/JAMC-D-12-0300.1, 2013.

Otieno, V. O. and Anyah, R. O.: CMIP5 simulated climate conditions of the Greater Horn of Africa (GHA). Part 1: Contemporary climate, Climate Dynamics, 41, 2081–2097, https://doi.org/10.1007/s00382-012-1549-z, 2013.

Palmieri, A., Annandale, G. W., Dinar, A., Johndrow, T. B., and Kawashima, S., Shah, F.: Reservoir conservation: economic and engineering evaluation of alternative strategies for managing sedimentation in storage reservoirs, The RESCON approach, 102, 2003.

Pohl, B., Crétat, J., and Camberlin, P.: Testing WRF capability in simulating the atmospheric water cycle over Equatorial East Africa, Climate Dynamics, 37, 1357–1379, https://doi.org/10.1007/s00382-011-1024-2, 2011.

Quenum, G. M. L. D., Arnault, J., Klutse, N. A. B., Zhang, Z., Kunstmann, H., and Oguntunde, P. G.: Potential of the Coupled WRF/WRF-Hydro Modeling System for Flood Forecasting in the Ouémé River (West Africa), Water (Switzerland), 14, https://doi.org/10.3390/w14081192, 2022.

Rasmussen, R., Ikeda, K., Liu, C., Gochis, D., Clark, M., Dai, A., Gutmann, E., Dudhia, J., Chen, F., Barlage, M., Yates, D., and Zhang, G.: Climate change impacts on the water balance of the Colorado headwaters: High-resolution regional climate model simulations, Journal of Hydrometeorology, 15, 1091–1116, https://doi.org/10.1175/JHM-D-13-0118.1, 2014.

Ryu, Y., Lim, Y. J., Ji, H. S., Park, H. H., Chang, E. C., and Kim, B. J.: Applying a coupled hydrometeorological simulation system to flash flood forecasting over the Korean Peninsula, Asia-Pacific Journal of Atmospheric Sciences, 53, 421–430, https://doi.org/10.1007/s13143-017-0045-0, 2017.

Sampson, K. and Gochis, D.: WRF Hydro GIS Pre-Processing Tools , Version 2 . 2 Documentation, 1–39, 2015.

Schaake, J. C., Koren, V. I., Duan, Q. Y., Mitchell, K., and Chen, F.: Simple water balance model for estimating runoff at different spatial and temporal scales, Journal of Geophysical Research Atmospheres, 101, 7461–7475, https://doi.org/10.1029/95JD02892, 1996.

Schmidli, J., Frei, C., and Vidale, P. L.: Downscaling from GCM precipitation: A benchmark for dynamical and statistical downscaling methods, International Journal of Climatology, 26, 679–689, https://doi.org/10.1002/joc.1287, 2006.

Schumacher, V., Fernández, A., Justino, F., and Comin, A.: WRF High Resolution Dynamical Downscaling of Precipitation for the Central Andes of Chile and Argentina, Frontiers in Earth Science, 8, https://doi.org/10.3389/feart.2020.00328, 2020.

Schwartz, C. S.: Reproducing the september 2013 record-breaking rainfall over the colorado front range with high-resolution WRF forecasts, Weather and Forecasting, 29, 393–402, https://doi.org/10.1175/WAF-D-13-00136.1, 2014.

Seck, A., Welty, C., and Maxwell, R. M.: Spin-up behavior and effects of initial conditions for an integrated hydrologic model, Water Resources Research, 51, 2188–2210, https://doi.org/10.1002/2014WR016371, 2015.

Senatore, A., Mendicino, G., Gochis, D. J., Yu, W., Yates, D. N., and Kunstmann, H.: Fully coupled atmosphere-hydrology simulations for the central Mediterranean: Impact of enhanced hydrological parameterization for short and long time scales, Journal of Advances in Modeling Earth Systems, 7, 1693–1715, https://doi.org/10.1002/2015MS000510, 2015.

Senior, C. A.: Convection permitting regional climate change simulations for understanding future climate and informing decision making in Africa in: Bulletin of the American Meteorological Society - Ahead of print, 2021.

Siderius, C., Biemans, H., Kashaigili, J. J., and Conway, D.: Going local: Evaluating and regionalizing a global hydrological model's simulation of river flows in a medium-sized East African basin, Journal of Hydrology: Regional Studies, 19, 349–364, https://doi.org/10.1016/j.ejrh.2018.10.007, 2018.

Skamarock, W. C., Klemp, J. B., Dudhia, J., Gill, D. O., Barker, D. M., Duda, M. G., Huang, X.-Y., Wang, W., and Powers, J. G.: A Description of the Advanced Research WRF Version 4, https://doi.org/10.6084/m9.figshare.7369994.v4, 2019.

Song, X. M., Kong, F. Z., Zhan, C. S., Han, J. W., and Zhang, X. H.: Parameter identification and global sensitivity analysis of Xin'anjiang model using meta-modeling approach, Water Science and Engineering, 6, 1–17, https://doi.org/10.3882/j.issn.1674-2370.2013.01.001, 2013.

Stratton, R. A., Senior, C. A., Vosper, S. B., Folwell, S. S., Boutle, I. A., Earnshaw, P. D., Kendon, E., Lock, A. P., Malcolm, A., Manners, J., Morcrette, C. J., Short, C., Stirling, A. J., Taylor, C. M., Tucker, S., Webster, S., and Wilkinson, J. M.: A Pan-African convection-permitting regional climate simulation with the met office unified model: CP4-Africa, Journal of Climate, 31, 3485–3508, https://doi.org/10.1175/JCLI-D-17-0503.1, 2018.

Tao, W., Huang, G., Lau, W. K. M., Dong, D., Wang, P., and Wen, G.: How can CMIP5 AGCMs' resolution influence precipitation in mountain areas: the Hengduan Mountains?, Climate Dynamics, 54, 159–172, https://doi.org/10.1007/s00382-019-04993-w, 2020.

Taye, M. T. and Dyer, E.: Hydrologic Extremes in a Changing Climate: a Review of Extremes in East Africa, Current Climate Change Reports, 10, 1–11, https://doi.org/10.1007/s40641-024-00193-9, 2024.

Taylor, K. E.: Summarizing multiple aspects of model performance in a single diagram, Journal of Geophysical Research Atmospheres, 106, 7183–7192, https://doi.org/10.1029/2000JD900719, 2001.

Taylor, R. G., Todd, M. C., Kongola, L., Maurice, L., Nahozya, E., Sanga, H., and Macdonald, A. M.: Evidence of the dependence of groundwater resources on extreme rainfall in East Africa, Nature Climate Change, 3, 374–378, https://doi.org/10.1038/nclimate1731, 2013.

Teutschbein, C. and Seibert, J.: Bias correction of regional climate model simulations for hydrological climate-change impact studies: Review and evaluation of different methods, Journal of Hydrology, 456–457, 12–29, https://doi.org/10.1016/j.jhydrol.2012.05.052, 2012.

Kenya Climate Change Case Study: https://www.trocaire.org/sites/default/files/resources/policy/kenya-climate-change-case-study.pdf, last access: 20 October 2024.

Wang, F., Ni, G., Riley, W. J., Tang, J., Zhu, D., and Sun, T.: Evaluation of the WRF lake module (v1.0) and its improvements at a deep reservoir, Geoscientific Model Development, 12, 2119–2138, https://doi.org/10.5194/gmd-12-2119-2019, 2019.

Wehbe, Y., Temimi, M., Weston, M., Chaouch, N., Branch, O., Schwitalla, T., Wulfmeyer, V., Zhan, X., Liu, J., and Al Mandous, A.: Analysis of an extreme weather event in a hyper-arid region using WRF-Hydro coupling, station, and satellite data, Natural Hazards and Earth System Sciences, 19, 1129–1149, https://doi.org/10.5194/nhess-19-1129-2019, 2019.

Wei, T.: A review of sensitivity analysis methods in building energy analysis, Renewable and Sustainable Energy Reviews, 20, 411–419, https://doi.org/10.1016/j.rser.2012.12.014, 2013.

Weusthoff, T., Ament, F., Arpagaus, M., and Rotach, M. W.: Assessing the benefits of convection-permitting models by neighborhood verification: Examples from MAP D-PHASE, Monthly Weather Review, 138, 3418–3433, https://doi.org/10.1175/2010MWR3380.1, 2010.

Williams, A. P. and Funk, C.: A westward extension of the warm pool leads to a westward extension of the Walker circulation, drying eastern Africa, Climate Dynamics, 37, 2417–2435, https://doi.org/10.1007/s00382-010-0984-y, 2011.

Yang, Z. L., Niu, G. Y., Mitchell, K. E., Chen, F., Ek, M. B., Barlage, M., Longuevergne, L., Manning, K., Niyogi, D., Tewari, M., and Xia, Y.: The community Noah land surface model with multiparameterization options (Noah-MP): 2. Evaluation over global river basins, Journal of Geophysical Research Atmospheres, 116, https://doi.org/10.1029/2010JD015140, 2011.

Yucel, I., Onen, A., Yilmaz, K. K., and Gochis, D. J.: Calibration and evaluation of a flood forecasting system: Utility of numerical weather prediction model, data assimilation and satellite-based rainfall, Journal of Hydrology, 523, 49–66, https://doi.org/10.1016/j.jhydrol.2015.01.042, 2015.

Zajac, Z., Revilla-Romero, B., Salamon, P., Burek, P., Hirpa, F., and Beck, H.: The impact of lake and reservoir parameterization on global streamflow simulation, Journal of Hydrology, 548, 552–568, https://doi.org/10.1016/j.jhydrol.2017.03.022, 2017.

Zandler, H., Haag, I., and Samimi, C.: Evaluation needs and temporal performance differences of gridded precipitation products in peripheral mountain regions., Scientific Reports, 9, https://doi.org/10.1038/s41598-019-51666-z, 2019.